Cancer Cell

Article

Retinoic acid receptor activation reprograms senescence response and enhances anti-tumor activity of natural killer cells

Graphical abstract

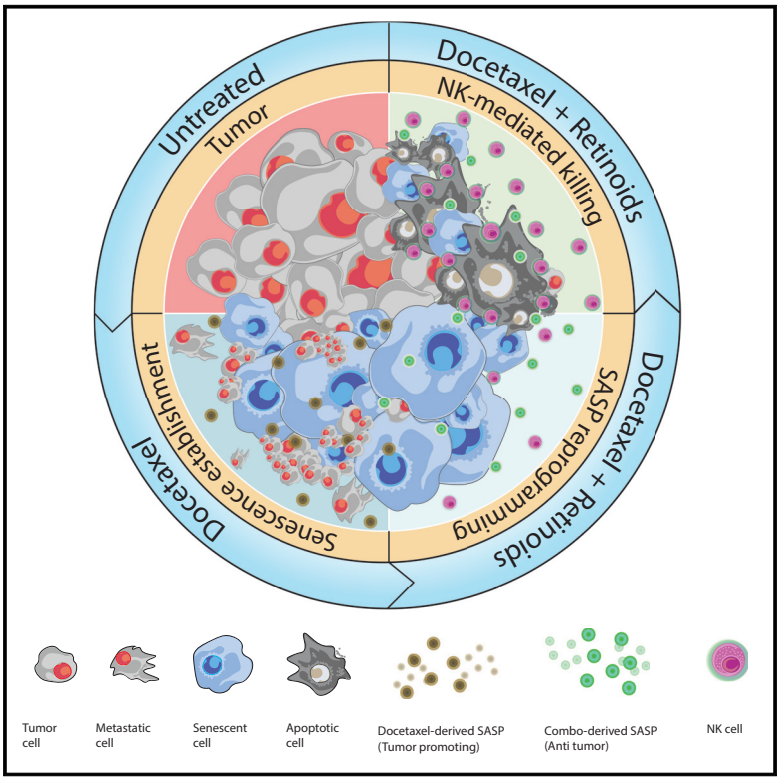

Authors

Manuel Colucci, Sara Zumerle, Silvia Bressan, Federico Gianfanti, ..., Bianca Calì, Monica Montopoli, Andrea Alimonti

Correspondence

andrea.alimonti@ior.usi.ch

In brief

Colucci et al. identify the RAR/RXR agonists as pro-senescence compounds triggering a potent p21-driven senescence response. The synergy of adapalene with docetaxel (Combo) mitigates the detrimental effects of docetaxel monotherapy. Finally, the antitumoral efficacy of the Combo treatment relies on the recruitment and activation of intratumoral natural killer cells.

Highlights

- Retinoids drive senescence in PCa
- PCa cells downregulate RA signaling and metabolism during progression
- Retinoids reprogram the SASP in docetaxel-treated tumors
- Senescence inducing compounds enhance the efficacy of allogenic NK infusion therapy

Colucci et al., 2024, Cancer Cell *42*, 646–661
April 8, 2024
https://doi.org/10.1016/j.ccell.2024.02.004

CellPress

CellPress
OPEN ACCESS

Cancer Cell

Article

Retinoic acid receptor activation reprograms senescence response and enhances anti-tumor activity of natural killer cells

Manuel Colucci,[1,2,3,20] Sara Zumerle,[4,20] Silvia Bressan,[1,2,5,20] Federico Gianfanti,[1,2,5,20] Martina Troiani,[1,2,6] Aurora Valdata,[1,7] Mariantonietta D'Ambrosio,[1,8] Emiliano Pasquini,[1,2] Angelica Varesi,[1,2] Francesca Cogo,[1,2] Simone Mosole,[1,2] Cristina Dongilli,[1,2] Maria Andrea Desbats,[4] Liliana Contu,[4] Ajinkya Revankdar,[9] Jingjing Chen,[10,11] Madhuri Kalathur,[12] Maria Luna Perciato,[13] Rossella Basilotta,[14] Laczko Endre,[15] Stefan Schauer,[15] Alaa Othman,[15] Ilaria Guccini,[7] Miriam Saponaro,[4] Luisa Maraccani,[1,5] Nicolò Bancaro,[1,2] Ping Lai,[1,2] Lei Liu,[1,2] Nicolò Pernigoni,[1,2] Federico Mele,[16] Sara Merler,[17] Lloyd C. Trotman,[18] Greta Guarda,[16] Bianca Calì,[1,2] Monica Montopoli,[5] and Andrea Alimonti[1,2,4,7,19,21,*]

[1]Institute of Oncology Research (IOR), CH6500 Bellinzona, Switzerland
[2]Università della Svizzera Italiana, CH6900 Lugano, Switzerland
[3]Faculty of Biology and Medicine, University of Lausanne UNIL, CH1011 Lausanne, Switzerland
[4]Veneto Institute of Molecular Medicine (VIMM) & Department of Medicine, University of Padova, Padova, Italy
[5]Veneto Institute of Molecular Medicine (VIMM) & Department of Pharmaceutical and Pharmacological Sciences, University of Padova, Padova, Italy
[6]Bioinformatics Core Unit, Swiss Institute of Bioinformatics, TI, Bellinzona, Switzerland
[7]Department of Health Sciences and Technology (D-HEST) ETH Zurich, Zurich, CH, Switzerland
[8]MRC London Institute of Medical Sciences (LMS), London, UK
[9]Massachusetts General Hospital Cancer Center, Harvard Medical School, Charlestown, MA 02129, USA
[10]Department of Cell Biology, Harvard Medical School, Boston, MA 02215, USA
[11]Department of Cancer Biology, Dana-Farber Cancer Institute, Boston, MA 02215, USA
[12]Children's GMP, LLC, St. Jude Children's Research Hospital, 262 Danny Thomas Place Mail Stop 920 Memphis, TN 38105, USA
[13]School of Clinical Dentistry, University of Sheffield, Sheffield S10 2TA, UK
[14]Department of Chemical, Biological, Pharmaceutical and Environmental Sciences, University of Messina, 98166 viale Ferdinando D'Alcontres, Italy
[15]Functional Genomics Center Zurich, ETHZ and University of Zurich, Zurich, CH, Switzerland
[16]Institute for Research in Biomedicine, Università della Svizzera Italiana, Bellinzona, Switzerland
[17]Section of Innovation Biomedicine - Oncology Area, Department of Engineering for Innovation Medicine, University of Verona and Verona University and Hospital Trust, Verona, Italy
[18]Cold Spring Harbor Laboratory, One Bungtown Road, Cold Spring Harbor, NY 11724, USA
[19]Oncology Institute of Southern Switzerland, Ente Ospedaliero Cantonale, Bellinzona, Switzerland
[20]These authors contributed equally
[21]Lead contact
*Correspondence: andrea.alimonti@ior.usi.ch
https://doi.org/10.1016/j.ccell.2024.02.004

SUMMARY

Cellular senescence can exert dual effects in tumors, either suppressing or promoting tumor progression. The senescence-associated secretory phenotype (SASP), released by senescent cells, plays a crucial role in this dichotomy. Consequently, the clinical challenge lies in developing therapies that safely enhance senescence in cancer, favoring tumor-suppressive SASP factors over tumor-promoting ones. Here, we identify the retinoic-acid-receptor (RAR) agonist adapalene as an effective pro-senescence compound in prostate cancer (PCa). Reactivation of RARs triggers a robust senescence response and a tumor-suppressive SASP. In preclinical mouse models of PCa, the combination of adapalene and docetaxel promotes a tumor-suppressive SASP that enhances natural killer (NK) cell-mediated tumor clearance more effectively than either agent alone. This approach increases the efficacy of the allogenic infusion of human NK cells in mice injected with human PCa cells, suggesting an alternative therapeutic strategy to stimulate the anti-tumor immune response in "immunologically cold" tumors.

INTRODUCTION

Prostate cancer (PCa) is the second leading cause of cancer-related mortality among men worldwide.[1,2] Standard chemotherapy can only marginally improve the overall patients' survival, providing a palliative benefit for patients who do not respond to androgen deprivation therapies.[3,4] We and others have shown that treatments that enhance senescence can initially suppress tumor growth.[5] Senescent tumor cells remain metabolically active and secrete a variety of cytokines and inflammatory factors in the tumor microenvironment (TME), known as the senescence-associated-secretory phenotype (SASP).[6,7] Interestingly, the SASP of tumor cells acts as a double-edged sword.[5,8,9] On the one hand, it prompts the immune system toward a robust clearance of the senescent cells.[8,10] On the other hand, it stimulates tumor cell growth, angiogenesis, metastasis, and therapy resistance.[11,12] Thus, if the tumor immune response does not remove senescent tumor cells, their persistence may cause tumor relapse and progression.[13,14] While several pro-senescence compounds have been discovered, their lack of efficacy and potentially harmful side effects significantly limit their clinical use.[11,15,16] In this respect, an effective pro-senescence therapy providing long-lasting benefits in cancer patients is still missing. Palbociclib, a potent inducer of senescence in tumor cells, has shown limited clinical efficacy in PCa.[17] Here, we took advantage of a broad chemogenomic screening platform to identify small molecules capable of triggering senescence in PCa cells.[18] Among different drugs, we identified the retinoic acid receptors (RARs) agonists as a potent class of pro-senescence compounds in PCa.

RARs belong to a subfamily of nuclear receptors (RARα, RARβ, and RARγ) involved in a wide range of pleiotropic effects spanning from cell growth, differentiation, survival, and homeostasis maintenance.[19–22] Upon dimerization with the retinoid X receptor (RXR), RARs work as transcription factors by binding to the retinoic acid response elements (RAREs) present in the promoter region of different target genes.[20,21,23] Nowadays, there are several available activators of the retinoic acid (RA) pathway, with the most effective compounds belonging to the third-generation retinoids (e.g., adapalene and bexarotene).[24–26] Third-generation retinoids are more chemically stable, less photolabile, and more lipophilic, allowing a more efficient cell entry.[19]

Therapeutically, we demonstrated that RAR agonists treatment in prostate tumor cells also enhanced senescence driven by docetaxel, a standard of therapy in PCa, switching the SASP of docetaxel from tumor-promoting into tumor-suppressive. Of note, this combination of compounds increased the intratumoral recruitment of natural killer (NK) cells and promoted NK cell-mediated tumor clearance. Conceptually, these results lay the foundation for combining allogenic NK cell-based immunotherapies with pro-senescence therapy in PCa patients.

RESULTS

RAR/RXR agonists induce senescence in prostate cancer cells

To identify pro-senescence compounds capable of enhancing senescence in prostate tumor cells, we took advantage of a chemogenomic screening platform previously developed in the laboratory.[18] The screening library accounted for more than 90,000 compounds. Among them, we prioritized the study of compounds either at an advanced stage of preclinical development or already used in the clinic (N = 500). The screening library included drugs developed for cancer, metabolic, and neurodegenerative diseases, some of which were FDA-approved, and compounds from the "library of pharmacologically active compounds" (LOPAC) (Figure S1A). Compounds were first screened in mouse embryonic fibroblasts (MEFs) for their efficacy and selectivity (Figure S1B) and later in both mouse (TrampC1, TrampC1$^{Pten-/-}$ and RapidCaP) and human (PC3, PC3shTIMP1, LNCaP, 22RV1, and LAPC4) prostate tumor cells (Figures 1A–1D, S1C, and S1D). Among the screened compounds, we identified three retinoids, adapalene, bexarotene, and acitretin, as the most effective pro-senescence compounds in both mouse and human prostate tumor cells. Treatment of prostate tumor cells with adapalene and bexarotene significantly reduced tumor cell growth and activated a strong senescence response, as visualized by the increased senescence associated-β-galactosidase (SA-β Gal) positivity *in vitro*, without inducing cell death (Figures 1E–1H, S1E, and S1F).[27–29] *In vivo* experiments in allograft (TrampC1 cells injected in C57BL/6 mice) and in xenograft (PC3 cells injected in NRG mice) models confirmed the induction of senescence in the tumors, as shown by the reduction of the tumor volume and increased SA-β Gal positivity (Figures S1G and S1H).

To gain more insights into the mechanism of senescence induction by retinoids in PCa cells, we measured the mRNA expression of canonical senescence markers in treated cells (p16, p21, and p27), observing a preferential upregulation of p21 in all the tested cell lines (Figures 1I–1L and S1I). This result aligns with a published observation, indicating that RAR/RXR-activating factors might control p21 expression.[30] To explore whether p21 induction by RAR agonists was directly responsible for the senescent phenotype, we took advantage of a small molecule capable of inhibiting p21 by decreasing its protein level (UC2288)[31,32] (Figure S1J). p21 inhibition prior to adapalene and bexarotene treatment nullified the pro-senescence properties of RAR/RXR activation in terms of proliferation arrest and SA-β Gal positivity (Figures 1M–1O and S1K). These results were confirmed at the genetic level using a shRNA against p21 (Figures S1L–S1N). The loss of p21 impaired the efficacy of adapalene and bexarotene, suggesting its central role in RAR/RXR-driven senescence. Taken together, these data demonstrate that RAR-RXR activation is a potent pro-senescence therapy for PCa. Moreover, mechanistically, the senescent phenotype dwells on the capacity of RARs to control p21, leading to a prompt arrest of the cell cycle and a persistent senescent state.

The retinol pathway and metabolism are impaired in PCa

To gain more insights into RA-associated signaling in PCa progression, we analyzed the modulation of different RA-associated gene datasets in RNA-seq data from more than 1,000 human prostate specimens. We used a published tool to stratify patients reporting a clustering progression from normal epithelium to the primary tumor, followed by castration-resistant prostate cancer (CRPC) and neuroendocrine (NE) tumors[33] (Figures 2A and 2B). We found that several pathways involved in RA signaling, activation of RA downstream targets, and RA metabolism were

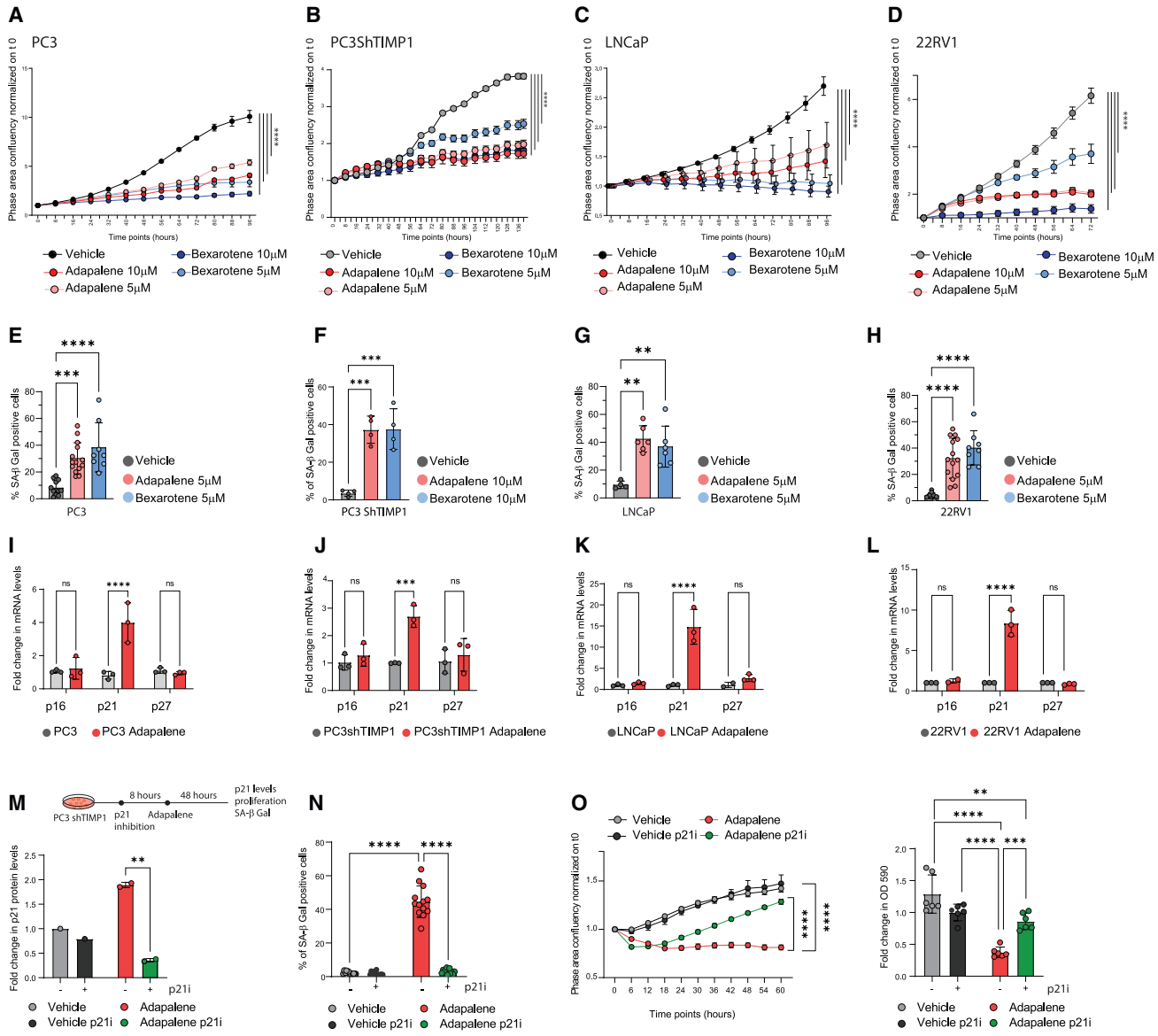

Figure 1. Identification of RAR agonists as pro-senescence compounds

(A) PC3 cell proliferation fold change with specified compounds, normalized to time 0.

(B) Fold change in PC3shTIMP1 cell proliferation treated with specified compounds, normalized to time 0.

(C) Fold change in LNCaP cell proliferation treated with specified compounds, normalized to time 0.

(D) Fold change in 22RV1 cell proliferation treated with specified compounds, normalized to time 0.

(E) SA-β Gal quantification in treated PC3 cells.

(F) SA-β Gal quantification in treated PC3shTIMP1 cells.

(G) SA-β Gal quantification in treated LNCaP cells.

(H) SA-β Gal quantification in treated 22RV1 cells.

(I) RT-qPCR analysis of senescence markers in PC3 cells.

(J) RT-qPCR analysis of senescence markers in PC3shTIMP1 cells.

(K) RT-qPCR analysis of senescence markers in LNCaP cells.

(L) RT-qPCR analysis of senescence markers in 22RV1 cells.

(M) Experimental design (upper panel) and western blot quantification (lower panel) of treated PC3shTIMP1 cells, referred to Figure S1J.

(N) SA-βGal quantification of PC3shTIMP1 cells treated with p21 inhibitor (p21i) UC2288 and adapalene.

(O) Fold change in proliferation normalized to time 0 of PC3shTIMP1 cells treated with the p21 inhibitor (p21i) UC2288 and adapalene (left panel) and cristal violet assay quantification (right panel). Data presented in (E–N) and (O, right) are shown as the mean ± SD; Data presented in (A–D) and (O, left) are presented as mean ± SEM. Data represent three to five independent experiments. Data presented in (M) represents one experiment. Statistical test used in data presented in (E–H): one-way ANOVA followed by Tukey's test *p < 0.05, **p < 0.01, ***p < 0.001, ****p < 0.0001. Statistical test used in data presented in (A–D) and (I–O): two-way ANOVA *p < 0.05, **p < 0.01, ***p < 0.001, ****p < 0.0001. Also see Figure S1.

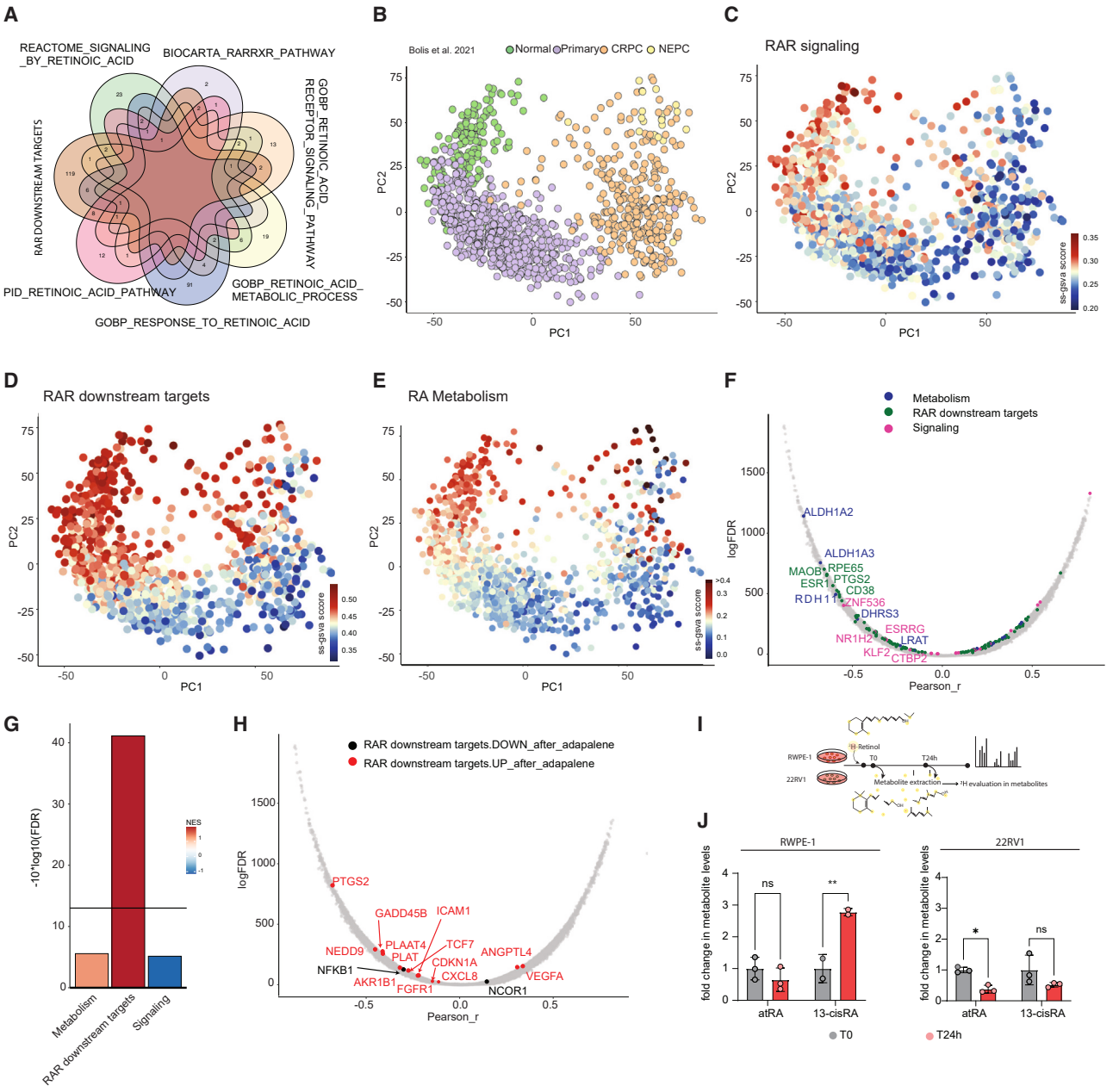

Figure 2. The retinol metabolism and pathway are impaired during PCa progression

(A) Venn diagrams depicting the number of differentially expressed genes in each RA-associated signature.

(B) Principal component analysis (PCA) of pan-prostate cancer transcriptomes obtained from the indicated studies of normal prostate (green), and primary (purple), castration-resistant (CRPC, orange), and neuroendocrine prostate cancer (NEPC, yellow).

(C) PCA showing the activation of RAR signaling pathway during PCa disease progression.

(D) PCA showing the expression of RAR downstream targets during PCa disease progression.

(E) PCA showing the expression of RA metabolism related genes during PCa disease progression.

(F) Plot representing the Pearson correlation of RA-related genes from RNA-seq data of patients. Gray dots represent genes not related to the RAR pathway, blue dots represent genes related to RA metabolism, green dots represent genes that are RAR targets, and pink dots represent genes related to the RAR signaling.

(G) Barplot showing the NES of RAR downstream targets, RA-associated metabolism and RAR signaling from RNA-seq of PC3shTIMP1 cells upon adapalene treatment compared to untreated cells.

(H) Plot representing the Pearson correlation of the RA-related genes from RNA-seq data of patients and PC3shTIMP1 cells treated with adapalene. Gray dots represent genes not related to the RAR pathway, black dots represent genes downregulated upon adapalene treatment, and red dots represent genes upregulated upon adapalene treatment.

(legend continued on next page)

strongly downregulated during cancer progression compared to normal tissues (Figures 2C–2E, S2A, and S2B). Human prostate tumor cells, commonly used in the laboratory for *in vitro* experiments, also presented a decreased activation of the RA downstream targets compared to normal prostate tissue as detected by RNA-seq (Figure S2C). Among the genes that negatively correlated with cancer progression in the RA signaling and downstream target signatures, we found MAOB, ESR1, and PTGS2, which also control cellular senescence.[34,35] Between the genes related to RA metabolism, we found ALDH1A2 and ALDH1A3 that control the conversion of retinal to RA (Figures 2F and S2D–S2J). To assess whether adapalene treatment could activate the RA pathways in prostate tumor cells, we took advantage of PC3 cells that exhibit a decreased RA signaling compared to normal cells (Figure S2C). Pathway analysis showed a strong upregulation of genes of the RAR downstream targets signature but not of the RA signaling and metabolism (Figure 2G). Moreover, we found that adapalene treatment increased a signature of cellular senescence, while cell cycle progression was downregulated in line with our results *in vitro* (Figures S2K and S2L). Of note, adapalene treatment in PC3 cells restored the transcription of PTGS2, FGFR1, p21, and CXCL8, while the levels of ALDH1A1, ALDH1A2, and ALDH1A3 did not change (Figure 2H).

In line with the gene expression data, metabolic analysis using ^{2}H-labelled retinol (ROH) in normal and PCa cells revealed that PCa cells could not convert ROH into its active metabolites (13-*cis* RA and *all-trans* RA) (Figures 2I and 2J). Moreover, the treatment with adapalene in PCa cells did not rectify the RA metabolic impairment (Figure S2M). In conclusion, adapalene-dependent RAR activation in PCa cells increases the downstream RA signaling without affecting the upstream ROH metabolism needed to convert ROH into its active forms.

RARs activation enhances the efficacy of docetaxel by increasing senescence and reprogramming the SASP

Docetaxel is a taxane used at a late stage in metastatic PCa patients who experience hormonal therapy failure.[36] In recent years, several reports have also demonstrated that docetaxel can be effective when administered to hormone naive metastatic PCa patients.[37,38] Like other chemo- and radiotherapies, docetaxel can induce a strong senescence response.[11,13,39] We, therefore, assessed whether RAR/RXR agonists could enhance the efficacy of docetaxel-induced senescence when administered in combination by using the human PCa cell line PC3shTIMP1. As previously shown, PC3shTIMP1 cells are characterized by higher migratory capacity, invasiveness, and resistance to docetaxel therapy compared to PC3 cells, making them a suitable model for studying aggressive PCa. These tumor cells, when treated with docetaxel, secrete various tumor-promoting factors, including FGF1, IGFBP5, MMP2, and MMP9, which ultimately contribute to therapy resistance and metastatic dissemination.[13] We tested different concentrations of the drugs in a synergistic proliferation assay (Figure S3A). We monitored the growth inhibition of cancer cells after 48 h of treatment and calculated the combination index (CI) to assess the drug synergism.[40,41] Briefly, a CI equal to 1 indicates an additive effect, a CI greater than 1 indicates antagonism, and a CI lower than 1 indicates synergism.[40,41] In PC3shTIMP1 cells, the combinatorial treatment of docetaxel + adapalene and docetaxel + bexarotene (Combo) efficiently reduced cell growth compared to the single treatments (CI = 0.74 and CI = 0.62, respectively) (Figure 3A). These results were also confirmed in 22RV1 cells (Figure S3B). The cell-cycle arrest induced by the Combo was also accompanied by a strong induction of senescence *in vitro* as measured by SA-β-Gal assay and RT-qPCR for different senescence markers. The combination of docetaxel + adapalene or bexarotene increased the percentage of senescent tumor cells from 30% to 60% and from 40% to 60%, respectively, compared to docetaxel alone in both PC3shTIMP1 and 22RV1 cells (Figures 3B, 3C, and S3C).

We next treated PC3shTIMP1 cells with docetaxel, adapalene, or the Combo for more than seven days to assess whether Combo-induced senescence was more endurable than docetaxel-induced senescence. While docetaxel initially arrested cell proliferation in a fraction of cells by inducing senescence, after ten days in culture, non-senescent cells started to proliferate again due to the effect of the SASP as previously reported (Figure 3D).[13,42] On the contrary, adapalene and Combo established a permanent senescence state, thus highlighting the long-lasting effects of the growth arrest triggered by RAR agonists in prostate tumor cells (Figure 3D).

Next, we characterized the SASP evoked by the Combo and the single treatments by performing RNA-seq followed by pathway analysis and a cytokines array on PC3shTIMP1 cells (Figures 3E, 3F, S3D, and S3E). Interestingly, and in line with previous findings,[13,42] we found that while docetaxel upregulated multiple tumor-promoting secreted factors, adapalene treatment reverted this phenotype. Among the most downregulated factors in Combo-treated cells, we found FGF, IL-6, IL-23, MMP9, and THBS1 that, as previously shown, can promote prostate tumor outgrowth and migration (tumor-promoting SASP)[13,43] (Figures 3F and S3E). Interestingly, the secretome of the Combo-treated cells was also enriched with many secreted factors linked to the activation of the anti-tumor immune response, such as IL-33, IL-15, MIG, and IL-12 (immune activating SASP) (Figures 3F and S3E).[44,45]

We next investigated the role of the SASP at the functional level by performing conditioned media (cm) experiments using PC3shTIMP1 cells treated with either docetaxel, adapalene, or Combo and untreated parental tumor cells (Figures 3G–3L). The cm from Docetaxel-treated cells increased the invasion, migration, and proliferation of parental untreated tumor cells.[13,42] However, these phenotypes were not observed in tumor cells treated with the cm of adapalene or the Combo (Figures 3G–3L). These results were further validated by coculturing RapidCaP cells pre-treated with docetaxel, adapalene, and the Combo in the presence of td-Tomato^{+} labeled parental untreated RapidCaP cells (Figure 3M). While docetaxel-treated

(I) Experimental design of (J).
(J) Fold change in ROH conversion products (atRA and 13-cisRA) in a non-transformed prostate cell line, RWPE-1, and a cancer cell line, 22RV1 upon ^{2}H-ROH exposure. Data presented in (J) are shown as the mean ± SD representing one experiment. Statistic test used in (J): one-way ANOVA followed by Tukey's test *p < 0.05, **p < 0.01, ***p < 0.001, ****p < 0.0001. See also Figure S2.

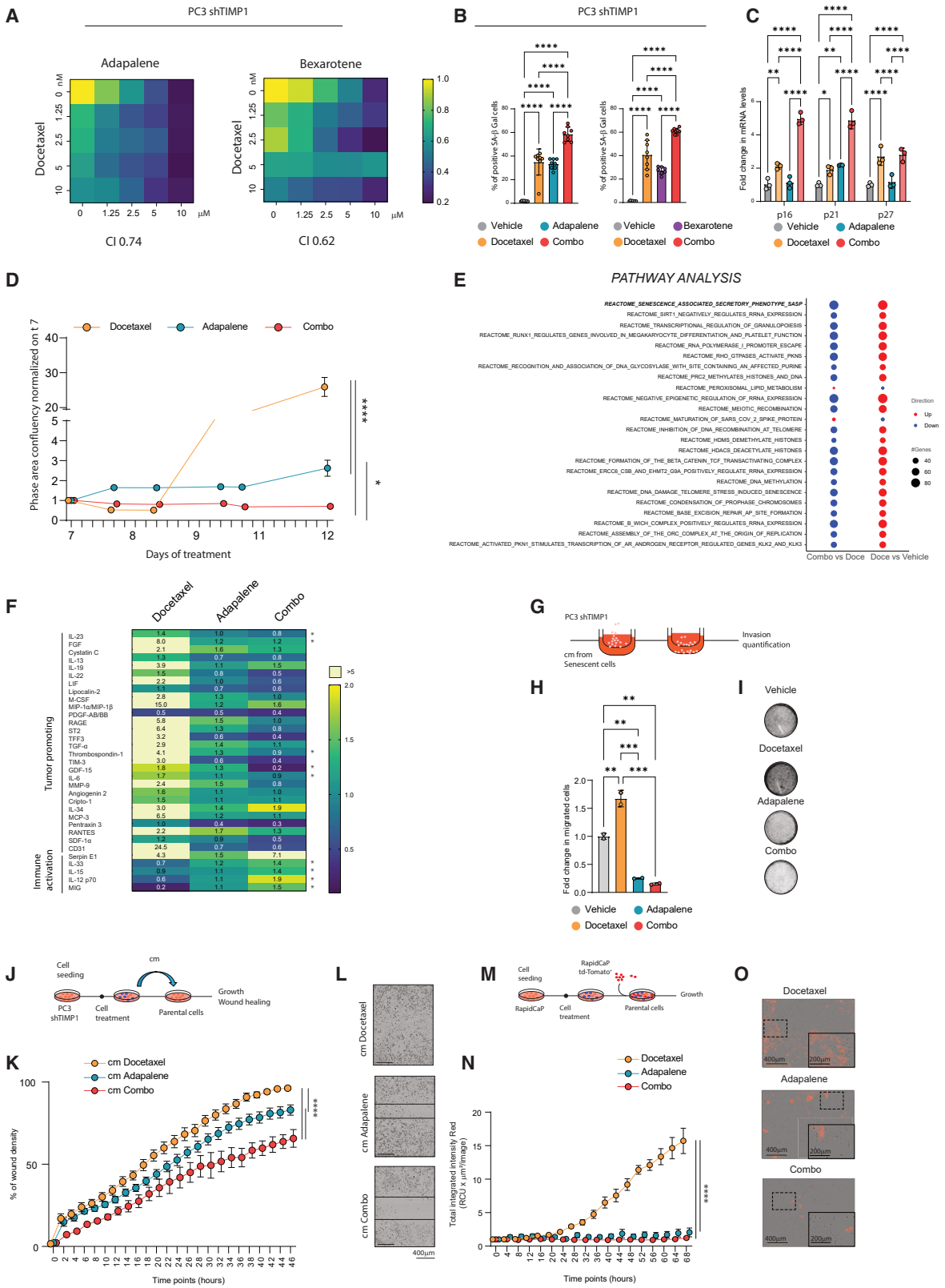

Figure 3. RARs activation enhances chemotherapy by reprogramming the SASP

(A) Heatmap showing the results of the synergistic proliferation assay performed on PC3shTIMP1 cells treated with the combination of either docetaxel and adapalene or docetaxel and bexarotene (48 h of treatment).

(legend continued on next page)

cells propelled the proliferation of td-Tomato$^+$ cells, adapalene and Combo-treated cells did not (Figures 3N and 3O). These data demonstrate that adapalene enhances senescence and reprograms the SASP of docetaxel-treated cells, thereby stably arresting tumor cell proliferation and mitigating the pro-tumorigenic effects of the docetaxel-driven SASP.

Adapalene treatment reprograms docetaxel-induced SASP by inhibiting AP-1

Intrigued by the capability of adapalene to revert the pro-tumorigenic SASP of docetaxel, we dug into the mechanisms that regulate the composition of the SASP by comparing the SASP of docetaxel and Combo treated cells. Between the factors upregulated by docetaxel but downregulated by Combo treatment (Figures 4A and 4B), we identified the transcription factors JUN, FOS, PRDM1, EGR1, ATF3, and TNFAIP3, all of which belong to the AP-1 family of transcription factors (Figure 4B).[46] Interestingly, AP-1 has been previously identified as a pioneer transcription factor upregulated in senescent cells.[42,47] Network analysis confirmed that JUN was the most interconnected transcription factor between the top upregulated factors in docetaxel-driven senescence, suggesting that it could be a possible regulator of all the other factors (Figure S4A). Therefore, we formed the hypothesis that AP-1 could control the tumor-promoting SASP of docetaxel, and this could be reverted by adapalene co-treatment.

First, we engineered PC3shTIMP1 cells to express a fluorescent reporter (mCherry) for AP-1 activity (Figure 4C).[48] While docetaxel treatment increased the mCherry signal, adapalene administration blocked the activation of AP-1 induced by docetaxel (Figures 4D and 4E).

We also validated the role of AP-1 inhibition in docetaxel-induced SASP by taking advantage of a known AP-1 inhibitor, T-5224 (Figures 4D and 4E).[49] Administration of T-5224 to prostate tumor cells treated with docetaxel, adapalene, or Combo did not affect senescence establishment (Figure 4F). Of note, AP-1 inhibition reverted the detrimental effects of the docetaxel-driven SASP on untreated parental prostate tumor cells, as assessed by tumor cell proliferation, migration, and SASP gene expression levels, thereby phenocopying the effect of adapalene (Figures 4G–4K and S4B). These findings were further validated using a selective JUN inhibitor (Juni) (Figures S4C–S4G). Conversely, overexpression of c-JUN in PC3shTIMP1 cells treated with docetaxel further increased the levels of the tumor-promoting SASP genes (Figures S4H–S4J). Taken together, these results show that the tumor-promoting SASP of docetaxel depends on AP-1. Inhibition of AP-1 by RAR agonists reprograms the SASP of docetaxel, preventing its harmful effects on neighboring tumor cells.

Adapalene, in combination with docetaxel, enhances senescence and activates an anti-tumor immune response

We next validated the efficacy of adapalene and docetaxel combinatorial treatment *in vivo*. We subcutaneously injected RapidCaP cells into C57BL/6 mice. When tumors reached a final volume of 100 mm^3, treatments were administered either in single or combination (Figure 5A). Combinatorial treatment of adapalene and docetaxel significantly reduced tumor growth, while single treatments showed a less pronounced effect (Figure 5B). At early time points, Combo-treated tumors showed a strong senescence response compared to single-treated tumors as detected by RT-qPCR, IHC, SA-β Gal, and western blot analysis for p21 (Figures S5A–S5D). At a late time point, combo-treated tumors also presented an upregulation of the cell death marker cleaved caspase 3 (CC3) by western blot and immunoflorescence (IF) (Figures 5C, 5D and S5E).

Given that the SASP induced by the Combo was enriched in cytokines capable of attracting and activating immune cells (Figures 3F and S3E), we next investigated whether such treatments could influence the tumor immune response. Thus, we performed FACS analysis to characterize the immune populations infiltrating the tumors of treated mice. We found that the

(B) Quantification of SA-β Gal assay performed in PC3shTIMP1 cells after two days of treatment with docetaxel, adapalene, and their Combo (left), and docetaxel, bexarotene, and their Combo (right).
(C) RT-qPCR analysis for the senescence markers in PC3shTIMP1 cells treated with docetaxel, adapalene, and the Combo.
(D) Fold change in PC3shTIMP1 cells proliferation normalized on day 7 in continuum treatment with the indicated drugs for 12 days (media refreshed every three days).
(E) Pathway analysis performed on the RNA-seq of PC3shTIMP1 cells, showing the upregulated and downregulated pathways in Combo vs. docetaxel and docetaxel vs. vehicle. Pathway reported with FDR <0.05.
(F) Cytokine array of PC3ShTIMP1 cells treated with the indicated drugs and normalized on the vehicle-treated cells.
(G) Experimental design of (H and I).
(H) Quantification of Boyden chamber migration assay performed on PC3shTIMP1 cells exposed to the cm of docetaxel, adapalene, or the Combo, expressed as fold change in OD590.
(I) Representative images of Boyden chambers stained with cristal violet.
(J) Experimental design of (K and L).
(K) Percentage of wound density of PC3shTIMP1 parental cells treated with conditioned media (cm) from docetaxel, adapalene, or Combo-treated PC3shTIMP1 cells.
(L) Representative pictures of K (scale bar: 400 μm).
(M) Experimental design of (N and O).
(N) Proliferation of TdTomato$^+$ RapidCaP cells cocultured with senescent non-labeled RapidCaP cells, quantified as fold change in total integrated intensity (RCU x μm^2/image).
(O) Representative images of the proliferation assay in N (scale bar: 400 μm, inserts 200 μm). Data presented in (B), (C), and (H) are shown as the mean ± SD. Statistic test used for (H): one-way ANOVA followed by Tukey's test *p < 0.05, **p < 0.01, ***p < 0.001, ****p < 0.0001. Data presented in (D), (K), and (N) are shown as the mean ± SEM. Statistic test used in (B–D), (K), and (N): two-way ANOVA *p < 0.05, **p < 0.01, ***p < 0.001, ****p < 0.0001. Data presented in (F) are representative of one experiment. Data shown in panels (A–D), (H), (K), and (N) are representative of three independent experiments. See also Figure S3.

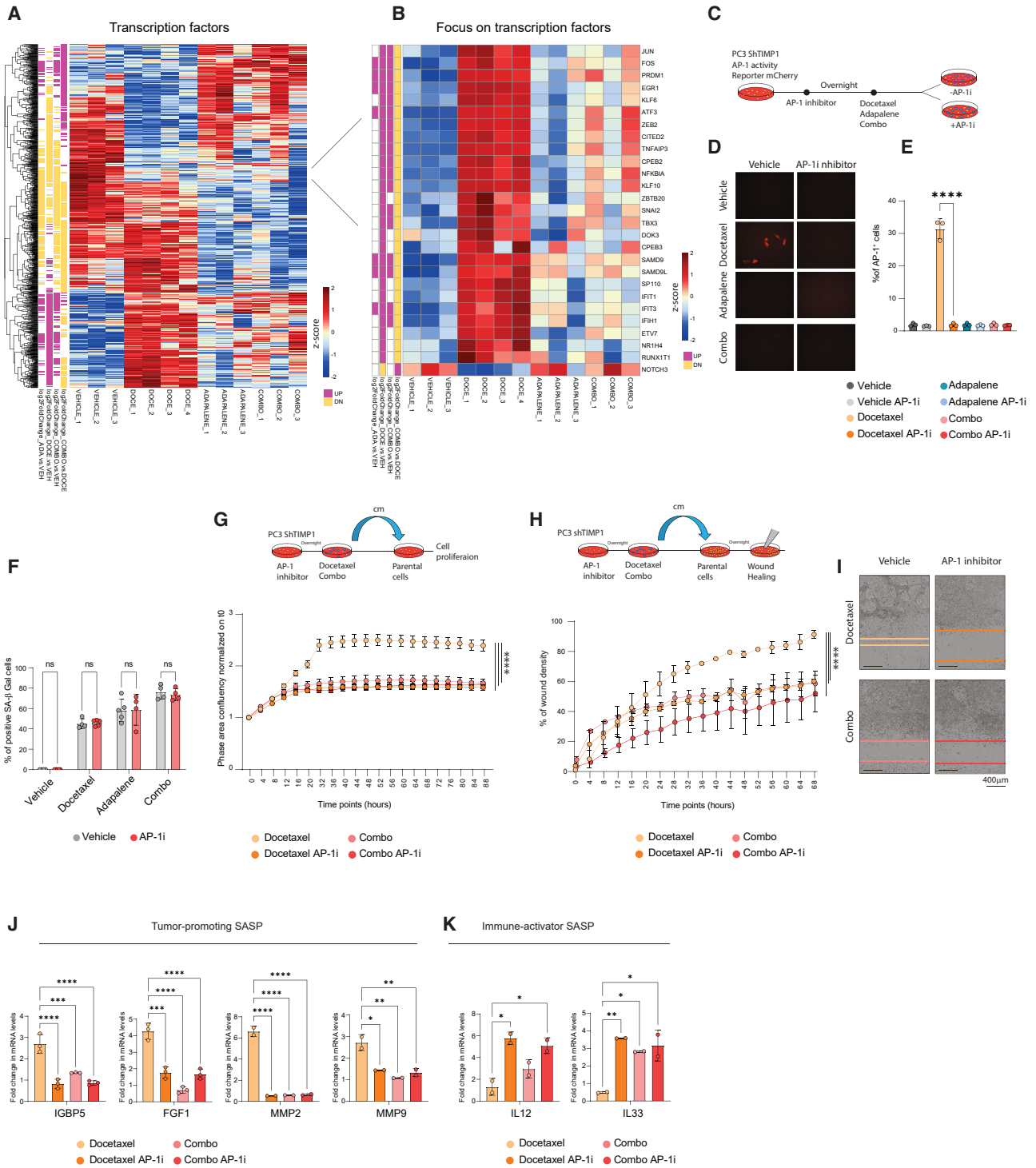

Figure 4. Adapalene reprograms the detrimental SASP triggered by docetaxel through AP-1

(A) Heatmap showing the differentially expressed transcription factors in PC3shTIMP1 cells treated with docetaxel, adapalene, and the Combo. Genes reported with FDR <0.05 in at least one comparison to the vehicle.

(B) Focus on the heatmap showing the differentially expressed transcription factors in PC3shTIMP1 cells having an opposite expression pattern in cells treated with docetaxel compared to vehicle and in the Combo compared to docetaxel.

(C) Schematic representation of (D and E).

(D) Representative pictures of AP-1-mediated transcriptional activition depicted as mCherry fluorescence.

(E) Quantification of mCherry positive PC3shTIMP1 cells upon docetaxel, adapalene, or Combo treatments in the presence or absence of the AP-1 inhibitor (AP-1i) T-5224.

(legend continued on next page)

percentage of NK, but not NKT cells, was enriched in Combo-treated prostate tumors compared to tumors untreated or treated with single drugs (Figures 5E–5H and S5F–S5I). In line with our data *in vitro* (Figures 3F and S3E), RT-qPCR analysis on total tumor lysates showed that tumors treated with the Combo, but not with the single treatments, upregulated several secreted factors that both recruit and activate NK cells such as IL-12, IL-15 and IL-33, three critical recruiters of NK cells[50–52] (Figures 5I and S5J). Increased tumor infiltration of NK cells was also associated with higher Interferon-γ and granzyme-B intratumor levels, suggesting that these immune cells were activated[53] (Figure 5I). Next, we co-treated RapidCaP-injected mice with the Combo in the presence of the NK1.1 blocking antibody. Of note, intratumoral depletion of NK cells partially rescued the anti-tumor effect of the Combo (Figure S5K). These data were further validated using the anti-Asialo-GM1 blocking antibody, which targets a glycolipid found on the surface of NK but not on NKT cells (Figures 5J–5L).[54] On the contrary, the depletion of $CD8^+$ T cells in tumor-bearing mice treated with the Combo was ineffective (Figure S5L). In sum, these data showed that the Combo treatment is a valuable pro-senescence therapy for cancer. On the one hand, it promotes a strong cellular senescence in prostate tumor cells; on the other hand, it drives a SASP that recruits NK cells, which mediate a substantial cytotoxic anti-tumor effect.

Adapalene, in combination with docetaxel, increases the anti-tumor activity of human NK cells

To corroborate the results obtained *in vivo* in a clinically relevant setting, we studied the interplay between senescent human tumor cells and human NK (hNK) cells. hNK cells were isolated from human PBMC and incubated with different human PCa cell lines (PC3, LNCaP, and 22RV1) treated with vehicle, docetaxel, adapalene, or the Combo to trigger cellular senescence (Figure 6A). As measured by cytotox emission, NK-mediated cell death significantly increased only in Combo-treated senescent cells. On the contrary, docetaxel or adapalene-treated cells were less efficiently killed by NK cells (Figures 6B–6E). To further understand whether this effect was mediated by the drug treatment, the SASP, or the NK-tumor cells interaction, we performed a co-culture experiment using PC3 cells and three different approaches (Figure 6F): (1) direct treatment of hNK cells with the different compounds, (2) treatment of hNK cells with the SASP of treated cells, and (3) directly co-culturing hNK cells with PC3 cells treated with the different compounds. Remarkably, we found a substantial killing of tumor cells only when hNK cells were cocultured with the Combo-treated cells (Figure 6G). Together, these data suggest that Combo-treatment can affect the levels of NK-activating and/or -inhibitory ligands. To validate this hypothesis, we performed gene expression profiling for multiple activating and inhibitory NK cell ligands in prostate tumor cells treated with different compounds. In Combo-treated cells, we found an upregulation of both MICA and ULBP2, two ligands of the NK group 2 member D protein (NKG2D) receptor, and downregulation of CEACAM1 and LECTIN, two inhibitory ligands binding to HAVCR2 and LAG3 (Figure 6H).[55] MICA, but not ULBP2, was also upregulated at the protein level, as demonstrated by FACS analysis on the same cells (Figures 6I and 6J). To functionally validate the role of NKG2D-mediated NK cell killing in our setting, we co-cultured hNK cells with tumor cells treated with the Combo in the presence or absence of a blocking antibody for NKG2D (anti-NKG2D) (Figure 6K). Treatment with the anti-NKG2D impaired hNK-cell-mediated death in prostate tumor cells treated with the Combo (Figure 6L).

Intrigued by these findings, we assessed whether senescence triggered by the combination of adapalene and docetaxel could enhance the efficacy of allogenic hNK cell therapy in mice injected with human prostate tumor cells. NRG mice, that do not possess functional NK cells, were challenged with PC3shTIMP1 cells and treated with vehicle, docetaxel, or the Combo. Two weeks after the treatment, mice were injected IP with 2.5 $x10^6$ hNK cells (Figure 6M). While in untreated or docetaxel-treated mice, infusion of hNK cells did not promote tumor regression, mice treated with the senescence-inducing combination of drugs showed a dramatic reduction in tumors volume, along with an increased percentage of tumor-infiltrating hNK cells (Figures 6N and 6O).

A migration assay performed by co-culturing prostate tumor cells treated with the different compounds and hNK cells showed an increased migration of hNK cells only in Combo-treated cells. This effect was partially abrogated by the knockdown of IL-33 and IL-12 in Combo-treated PC3 cells (Figures S6A–S6C).

Collectively, these results demonstrate that the SASP of Combo-treated tumor cells increases the intratumoral recruitment of NK cells while the upregulation of MICA on senescent tumor cells mediates the activation of NK cells. These data pave the way to the clinical implementation of allogenic NK cell-based immunotherapies in PCa patients treated with immune-activating pro-senescence regimens.

DISCUSSION

Cellular senescence is a complex biological process characterized by tumor-suppressive features, which can be exploited as therapeutic target for cancer treatment.[5,8,56] During the last

(F) Quantification of SA-β Gal staining of PC3shTIMP1 cells treated with docetaxel, adapalene, or the Combo in the presence or absence of the AP-1i.
(G) Representation of the experimental design (upper panel) and fold change in proliferation of PC3shTIMP1 cells treated with the cm of prostate tumor cells treated with docetaxel or the Combo in the presence or absence of the AP-1i, normalized on t0 (lower panel).
(H) Experimental design (upper panel) and wound confluence (%) of PC3shTIMP1 cells treated with the cm of cells treated with docetaxel and the Combo (lower panel).
(I) Representative pictures of the wound healing assay of (H) (scale bar: 400 μm).
(J) Fold change in mRNA levels of the indicated tumor-promoting secreted factors.
(K) Fold change in mRNA levels of different activators of the anti-tumor immune response. Data presented in (G) and (H) are shown as mean ± SEM. Statistic test used: two-way ANOVA, ****$p < 0.0001$. Data are representative of three independent experiments. Data presented in (E), (F), (J), and (K) are shown as mean ± SD. Statistic test used in (E): one-way ANOVA followed by Tukey's test *$p < 0.05$, **$p < 0.01$, ***$p < 0.001$, ****$p < 0.0001$. Data presented in (F–H), (J), and (K): two-way ANOVA *$p < 0.05$, **$p < 0.01$, ***$p < 0.001$, ****$p < 0.0001$. Data represent two independent experiments. See also Figure S4.

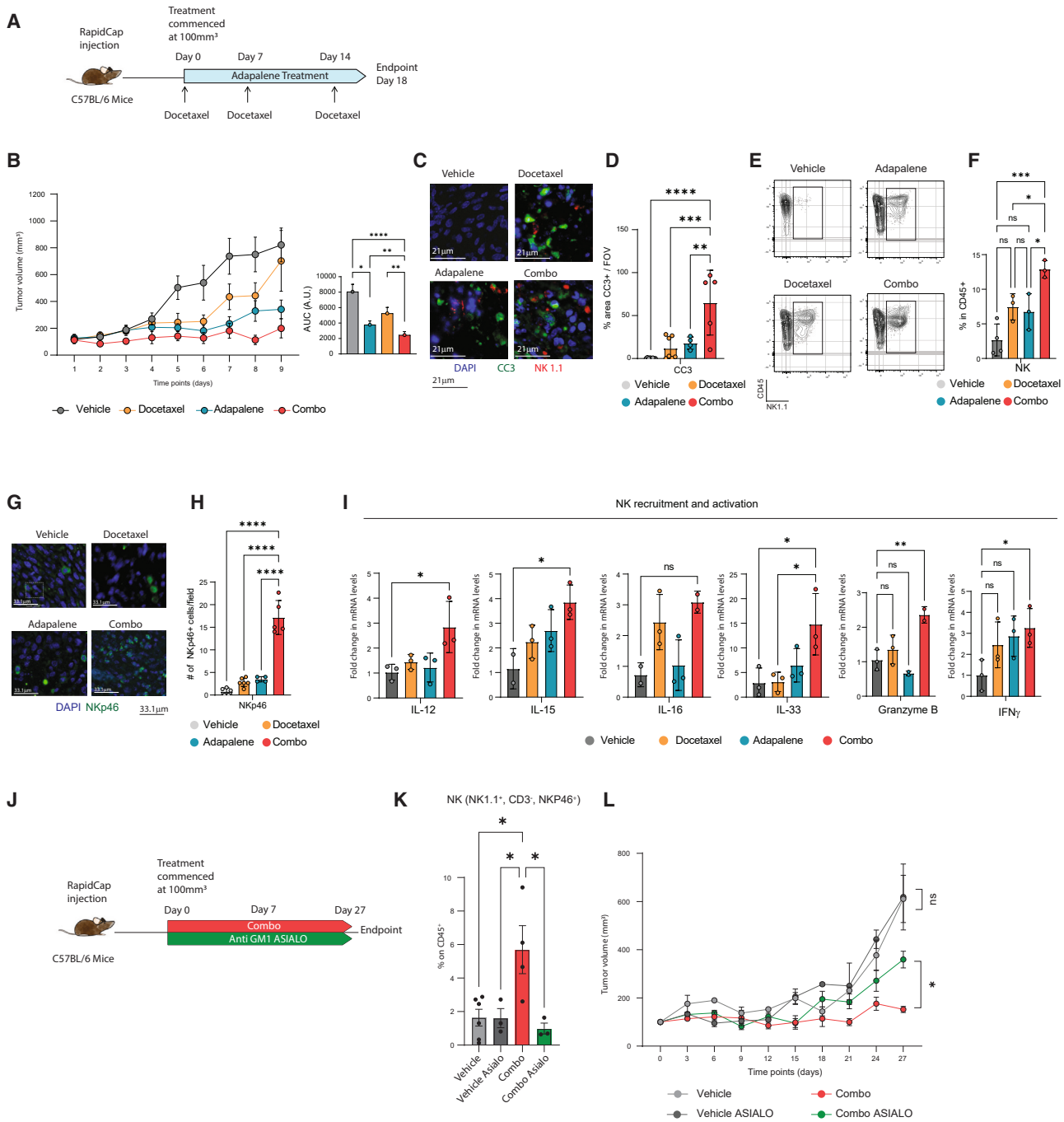

Figure 5. Adapalene, in combination with docetaxel, enhances senescence and activates an anti-tumor immune response

(A) Experimental design.

(B) Tumor volume in mm^3 of mice treated with the indicated drugs (n = 5 for each group) (left), and area under the curve calculated on tumor volume (right).

(C) Immunofluorescence staining for NK cells (by using anti NK1.1 antibody, in red) and cleaved caspase 3 (CC3, in green) in tumor sections (scale bar: 21 µm).

(D) Quantification of CC3 positive cells for field in tumors sections from (C).

(E) FACS plot for NK1.1 and $CD45^+$ cells gated in live cells in tumors treated with the indicated drugs.

(F) Percentage of $NK1.1^+$ cells in tumors treated with the indicated drugs.

(G) Immunofluorescence staining for NK cells (by using anti NKp46 antibody, in green) in tumor sections (scale bar: 33.1 µm).

(H) Quantification of NK cells for field in tumors sections from (G).

(I) Fold change in mRNA levels of recruiting factors for NK cells and granzyme B and IFNγ in tumors treated with the indicated drugs.

(J) Schematic representation of the experimental design of (K and L).

(K) Percentage of tumor-infiltrating NK cells ($NK1.1^+$, $CD3^-$, $NKp46^+$) gated in $CD45^+$ cells in tumors of mice untreated or treated with Combo and the Anti-GM1 Asialo.

(legend continued on next page)

decade, evidence has been provided regarding the ability of chemotherapies and targeted therapies to induce cellular senescence in cancer.[5,13,39,40,42,57,58] Although stably arrested, senescent cells are metabolically active and can support tumor progression by releasing a pro-inflammatory and pro-tumorigenic SASP.[6,7,10,59–61] We and others have demonstrated that the persistence of senescent tumor cells in the TME results in an increased inflammatory state, which drives tumor cell proliferation, migration, and even metastasis formation.[7,13,39,42] Thus, while the induction of senescence in cancer can be initially beneficial for tumor suppression, it results in tumor progression and treatment relapse at later stages of the disease.[5,8,56,62]

In this work, we identified a class of clinically available compounds that can potentially trigger a senescence response devoid of the detrimental effects of senescence cells. The chemogenomic screening we performed identified three potent senescence inducers, namely adapalene, acitretin, and bexarotene, all of which belong to the RAR/RXR agonists superfamily.[25,27,29] We focused on adapalene and bexarotene, two compounds of the third-generation retinoids/rexinoids, showing fewer off-target and side effects compared to the previous generations of drugs.[26,27] Adapalene and bexarotene are currently used in the clinic to treat mild-to-severe acne (*acne vulgaris*) and as an antineoplastic agent for T cell lymphoma, respectively.[24–28] They have different molecular target: adapalene preferentially binds to RAR-beta and RAR-gamma receptors (RARβ and RARγ), while bexarotene has a high selectivity for RXRs.[25,27,28] Upon homo- or hetero-dimerization, RARs/RXRs receptors bind to the DNA and modulate the transcriptional activity of target genes.[19–22] In this respect, the complex can recruit either co-activator or co-repressor proteins depending on the presence or absence of the ligand RA. Previous studies have highlighted a possible connection between RAR/RXR activation and p21 expression.[30] In agreement with these findings, we identified a significant upregulation of p21 in different cancer cell lines treated with the RAR agonists. This upregulation also correlated with a strong senescence response in the tested cell lines, thus suggesting a pivotal role of p21 in RAR agonist-mediated senescence. To further validate this hypothesis, we used a commercially available p21 inhibitor and a p21 sh-RNA.[32] Treatment with these compounds resulted in the impairment of senescence in adapalene-treated PCa cells.

To gain more insights into RA-associated signaling in PCa, we analyzed available RNA-seq data of PCa on more than 1,000 patients at different stages of the disease.[33] Interestingly, we observed that all the RA-associated signatures markedly decreased along with cancer progression. Adapalene treatment in PC3 cells restored the levels of several RAR downstream target genes, including genes involved in cellular senescence and cell cycle inhibition. However, it did not affect the expression of genes involved in the RA metabolism.

In vitro analysis showed that human PCa cell lines were less efficient than normal prostate cells in converting ROH into its mature form and that adapalene treatment did not rectify this metabolic defect. This aligns with a previous observation showing that PCa cells have lower RA levels than normal prostate tissues.[63]

To further analyze the therapeutic potential of RAR agonists, we tested them in combination with docetaxel, a gold standard for chemotherapy in PCa. Docetaxel has shown an effective improvement in the survival of PCa patients without granting long-lasting effects, as demonstrated by the high incidence of treatment resistance and tumor relapse.[37] In this respect, we recently showed that the accumulation of senescent tumor cells driven by docetaxel administration can favor metastasis formation in a mouse model of PCa characterized by combined loss of *Pten* and *Timp1*.[13,42] We demonstrated that, in this model, metastasis formation is mediated by the accumulation of senescent cells and that senolytic treatment significantly reduces the metastatic burden.[13,42] We also proved evidence that docetaxel-induced senescence is associated with the release of factors that promote the migration, invasion, and metastasis formation of neighboring non-senescent tumor cells.[7,13,42]

In this work, we reported that combining RAR agonists with docetaxel was more effective than the single treatments in reducing cell proliferation and inducing cellular senescence also in this model. By comparing the secretome induced by docetaxel alone or by the Combo, we also unexpectedly observed a different SASP composition. In Combo-treated cells, we reported a marked downregulation of factors involved in tumor cell proliferation and migration (FGF, IL-6, IL-23, MMPs, and FGF)[13] and a strong upregulation of factors activating the innate immune response (IL-12, MIG, IL-33, and IL-15).[44,45]

The analysis of RNA-seq data of PCa cells treated with the single drugs or the Combo also revealed profound changes in the expression of transcription factors involved in the regulation of the SASP. In particular, we observed that docetaxel treatment increased the expression levels of AP-1 transcription factors.[47] We also demonstrated that the detrimental effects of the docetaxel-driven SASP in PCa cells were abolished upon AP-1 inhibition or exacerbated upon AP-1 overexpression, pointing at AP-1 as a regulator of the detrimental SASP of docetaxel. On the contrary, in Combo-treated cells, we found a significant down-regulation of AP-1. This explains why the SASP of Combo-treated cells did not promote the proliferation and migration of non-senescent tumor cells in a co-culture experiment.

To further validate our findings, we moved to *in vivo* models. We demonstrated that the combination of docetaxel and adapalene effectively reduced the tumor burden while inducing the recruitment of anti-tumor NK cells. NK cells were partially responsible for the *in vivo* anti-tumor effect of the drug combination, as its efficacy was reduced upon the selective depletion of

(L) Tumor volume in mm^3 of mice treated with the indicated drugs in the presence or absence of the depleting antibody for NK cells (Vehicle, Iso n = 4, Vehicle, Asialo n = 4, Combo, Iso n = 3, Combo, Asialo n = 4). Data presented in (B) and (L) are shown as mean ± SEM. Statistic test used: two way ANOVA *$p < 0.05$, **$p < 0.01$, ***$p < 0.001$, ****$p < 0.0001$. Data in (B) are representative of two independent experiments. Data presented in (L) are representative of one experiment. Data presented in (D), (F), (H), (I), and (K) are shown as mean ± SD. Statistic test used: one-way ANOVA followed by Tukey's test *$p < 0.05$, **$p < 0.01$, ***$p < 0.001$, ****$p < 0.0001$. Data represent one experiment. See also Figure S5.

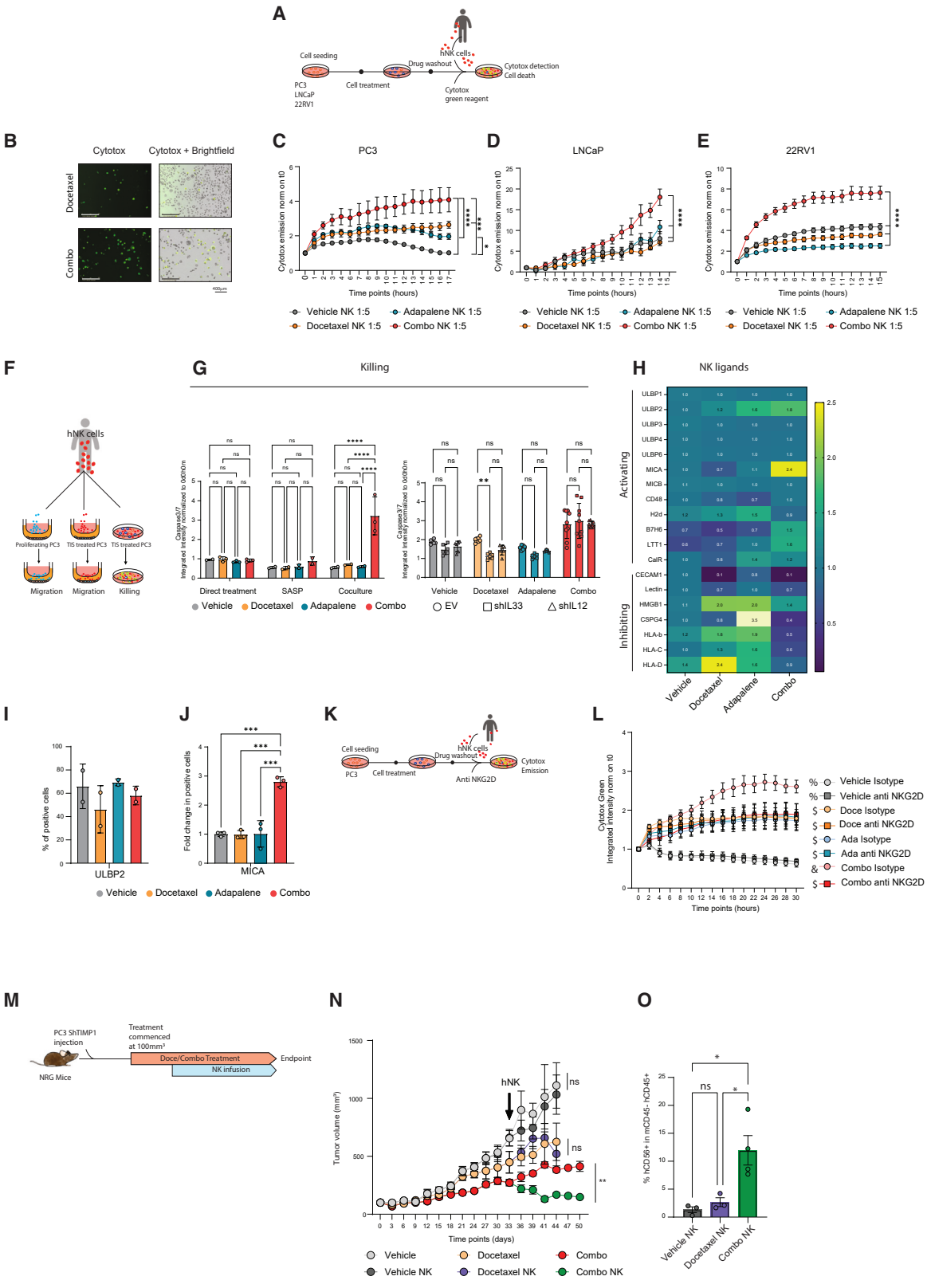

(legend on next page)

NK cells. Moreover, NK cells isolated from human buffy coats co-cultured with Combo-treated PCa cells were highly activated and characterized by a more substantial cytotoxic potential *in vitro* and *in vivo* than tumor cells treated with docetaxel and adapalene alone. We also demonstrated that this effect was mediated by the upregulation of MICA in prostate tumor cells treated with the Combo. MICA is an activatory NK ligand that specifically binds to the NKG2D receptor.[64] Inhibition of NKG2D in NK cells resulted in an impaired clearance of tumor cells in Combo-treated cells. Of note, the levels of many NK inhibitory receptors was also downregulated in cells treated with the Combo.

Finally, we found that the SASP of Combo-treated cells enhanced the recruitment of hNK cells in a co-culture experiment via IL-33 and IL-12. Taken together, these data demonstrate that the combination of adapalene and docetaxel-promotes both cell-autonomous and non-cell-autonomous anti-cancer effects.

Many efforts are emerging to develop and engineer NK cell-based cancer immunotherapy. Some clinical trials have demonstrated the overall safety of allogeneic NK cells in different cancer patients.[5,7,8] The feasibility of utilizing allogeneic NK cells and the established safety profiles have led to the development of ''off-the-shelf'' NK cell-based cancer immunotherapy. However, there are many challenges linked to the clinical use of these cell-based immunotherapies, such as a limited capability of NK cells *ex vivo* expansion, reduced *in vivo* persistence and infiltration, and poor NK cells activation. Various strategies are being employed to overcome these challenges, such as *ex vivo* pre-conditioning with cytokines, treatment with small molecules, NK cells engineering, or iPSC differentiation in NK cells.[47,63,65] In this respect, we envision that the combination of adapalene and docetaxel may be used as an alternative strategy to enhance the efficacy of allogenic infusion of NK cells or CAR-NK cell treatment in metastatic PCa patients. This combination of compounds could promote an increased migration of NK cells in the tumors, ultimately enhancing their antitumor activity in this cold tumor model.

STAR★METHODS

Detailed methods are provided in the online version of this paper and include the following:

- KEY RESOURCES TABLE
- RESOURCE AVAILABILITY
  - Lead contact
  - Materials availability
  - Data and code availability
- EXPERIMENTAL MODEL AND STUDY PARTICIPANT DETAILS
  - Mouse models
  - Prostate cancer cell culture
- METHOD DETAILS
  - *In vivo* treatments
  - Generation of a shTIMP1 human prostate cancer cell line
  - Generation of a shp21 cell line
  - Generation of a shIL-12 and IL-33 human prostate cancer cell Line
  - Generation of a cJUN overexpressing human prostate cancer cell line
  - Generation of PC3 shTIMP1 with mCherry reporter for AP-1
  - Generation of *Pten*$^{-/-}$ TrampC1 murine prostate cancer cell lines
  - Generation of mouse embryonic fibroblasts primary cell culture

Figure 6. RAR agonist in combination with docetaxel potentiates the anti-tumor activity of human-derived NK cells

(A) Experimental design.

(B) Representative images showing cytotox emission (in green) of PC3 cells pre-treated with docetaxel and Combo and co-cultured with human NK cells (scale bar: 400μm).

(C) Quantification of cytotox emission expressed as fold change in total integrated intensity (GCU x μm^2/image) of PC3 cells pre-treated with the indicated compounds and co-cultured with human NK cells (target:effector 1:5 ratio).

(D) Quantification of cytotox emission expressed as fold change in total integrated intensity (GCU x μm^2/image) of LNCaP cells pre-treated with the indicated compounds and co-cultured with human NK cells (target:effector 1:5 ratio).

(E) Quantification of cytotox emission expressed as fold change in total integrated intensity (GCU x μm^2/image) of 22RV1 cells pre-treated with the indicated compounds and co-cultured with human NK cells (target:effector 1:5 ratio).

(F) Schematic representation of the experimental layout of (G).

(G) Caspase 3/7 integrated intensity emission normalized on time 0 (t0) in PC3 cells treated with the indicated compounds (left) and engineered with different shRNAs: EV (circle), shIL-33 (square), and ShIL-12 (triangle), (right).

(H) RT-qPCR analysis in PC3 cells showing the expression of NK ligands on the cancer cells.

(I) FACS analysis showing the percentage of positive PC3 cells expressing ULBP2.

(J) FACS analysis showing the percentage of positive PC3 cells expressing MICA.

(K) Schematic representation of the experimental design of (L).

(L) Cytotox green emission integrated intensity normalized on time 0 (t0) in PC3 cells treated with the indicated compounds in the presence or absence of neutralizing antibody against NKG2D.

(M) Representation of the experimental design of (N and O).

(N) Tumor volume in mm^3 of mice treated with vehicle (n = 15), vehicle+NK (n = 16), docetaxel (n = 7), docetaxel+NK (n = 7), Combo (n = 15), Combo+NK (n = 16). Mice from vehicle, vehicle NK, docetaxel, and docetaxel NK were euthanized at an earlier time point (day 44) because of tumor ulceration.

(O) FACS analysis showing the percentage of hCD56$^+$ cells gated in hCD45$^+$, mCD45$^-$. Data presented in (G), (I), (J), and (O) are shown as mean ± SD. Data presented in (C–E), (L), and (N) are shown as mean ± SEM. Statistic test used in (C–E), (G), and (N): two-way ANOVA *p < 0.05, **p < 0.01, ***p < 0.001, ****p < 0.0001. Statistic test used in (I) and (J): one-way ANOVA followed by Tukey's test ***p < 0.001. Data presented in (C–E), (G–J), (L), and (N) represent two independent experiments. Data presented in (O) represent one experiment. Statistic test used in (L): two-way ANOVA. Lines with different symbols are statistically different from each other. See also Figure S6.

- Generation of Pten$^{-/-}$ MEFs
- *In vitro* treatments
- Drug combination assay
- Immunofluorescence (IF) assay
- Senescence Associated β-Galactosidase (SA-β Gal) assay
- Proliferation and cell death assay
- Cristal Violet assay
- Migration assay
- Invasion assay (Boyden chamber)
- Conditioned media assay
- Cytokine array
- Co-culture experiments
- Characterization of the tumor immune microenvironment
- NK cells isolation and coculture
- Isotope labeling and targeted Lipidomics
- Sample preparations and LC-MS methods
- LC-HRMS, fullMS1
- *MS method*
- LC-HRMS, parallel reaction monitoring (PRM)
- Liquid-liquid extraction
- LC-HRMS, fullMS1
- LC-HRMS, parallel reaction monitoring (PRM)
- LC-MS on a triple-quadrupole, selected reaction monitoring (SRM)
- MS method
- Western blot
- Antibodies
- RNA extraction and RNA sequencing (RNA-seq)
- Quantitative real-time PCR (RT-qPCR)
- Bioinformatic analysis

● QUANTIFICATION AND STATISTICAL ANALYSIS

SUPPLEMENTAL INFORMATION

Supplemental information can be found online at https://doi.org/10.1016/j.ccell.2024.02.004.

ACKNOWLEDGMENTS

We acknowledge all the members of Prof. Alimonti's laboratory, IOR/IRB/VIMM institutes, USI, UNIL, ETH and UNIPD universities. This work was supported by European Research Counsil (CoG 683136) https://cordis.europa.eu/project/id/683136, Swiss Cancer League (KFS-4267-08-2017, RWP-4813-06-2019, and KFS-5262-02-2021), SNSF (176045, 201274, and 202302), AIRC (IG 22030). S.Z. was supported by Fondazione Umberto Veronesi (Fellowship 2022). We acknowledge Marianna Sabbadin.

AUTHOR CONTRIBUTIONS

Conceptualization, A.A., M.C., S.Z., S.B., and F.G. Methodology, M.C., S.Z., S.B., and F.G. Software, M.T. Validation, M.C., S.Z., S.B., and F.G. Formal Analysis, M.C., S.Z., S.B., F.G., and M.T. Investigation, M.C., S.Z., S.B., F.G., A. Valdata, A. Varesi, M.D.A, F.C., M.S. S.Mosole., E.P., M.A.B.., R.B., M.L.P., C.D., L.C., L.M., S.Merler., L.E., S.S., and A.O. Resources, A.R., B.C., F.M., N.P., N.B., P.L., L.L., J.C., M.K., M.L.P., I.G., M.D.An., L.C.T, and M.M. Writing – original draft, A.A. and M.C. Writing – review & editing, A.A., M.C., S.Z., F.G., M.T., S.B., A. Valdata, and B.C. Visualization, M.C., S.Z., S.B., F.G., and M.T. Supervision, M.C., and S.Z. Funding Acquisition: A.A. and S.Z.

DECLARATION OF INTERESTS

A.A. is a co-founder of and owns stock in OncoSense, and A.A., M.C., and A.R. are inventors of the patent WO2019142095A1 (Title: new alk inhibitor senolytic drugs).

Received: May 17, 2023
Revised: December 19, 2023
Accepted: February 7, 2024
Published: February 29, 2024

REFERENCES

1. Rebello, R.J., Oing, C., Knudsen, K.E., Loeb, S., Johnson, D.C., Reiter, R.E., Gillessen, S., Van der Kwast, T., and Bristow, R.G. (2021). Prostate cancer. Nat. Rev. Dis. Prim. *7*, 9. https://doi.org/10.1038/s41572-020-00243-0.
2. Litwin, M.S., and Tan, H.J. (2017). The Diagnosis and Treatment of Prostate Cancer: A Review. JAMA *317*, 2532–2542. https://doi.org/10.1001/jama.2017.7248.
3. Tannock, I.F., de Wit, R., Berry, W.R., Horti, J., Pluzanska, A., Chi, K.N., Oudard, S., Théodore, C., James, N.D., Turesson, I., et al. (2004). Docetaxel plus prednisone or mitoxantrone plus prednisone for advanced prostate cancer. N. Engl. J. Med. *351*, 1502–1512. https://doi.org/10.1056/NEJMoa040720.
4. Petrylak, D.P., Tangen, C.M., Hussain, M.H.A., Lara, P.N., Jr., Jones, J.A., Taplin, M.E., Burch, P.A., Berry, D., Moinpour, C., Kohli, M., et al. (2004). Docetaxel and estramustine compared with mitoxantrone and prednisone for advanced refractory prostate cancer. N. Engl. J. Med. *351*, 1513–1520. https://doi.org/10.1056/NEJMoa041318.
5. Zumerle, S., and Alimonti, A. (2020). In and out from senescence. Nat. Cell Biol. *22*, 753–754. https://doi.org/10.1038/s41556-020-0540-x.
6. Coppé, J.P., Patil, C.K., Rodier, F., Sun, Y., Muñoz, D.P., Goldstein, J., Nelson, P.S., Desprez, P.Y., and Campisi, J. (2008). Senescence-associated secretory phenotypes reveal cell-nonautonomous functions of oncogenic RAS and the p53 tumor suppressor. PLoS Biol. *6*, 2853–2868. https://doi.org/10.1371/journal.pbio.0060301.
7. Coppé, J.P., Desprez, P.Y., Krtolica, A., and Campisi, J. (2010). The senescence-associated secretory phenotype: the dark side of tumor suppression. Annu. Rev. Pathol. *5*, 99–118. https://doi.org/10.1146/annurev-pathol-121808-102144.
8. Muñoz-Espín, D., and Serrano, M. (2014). Cellular senescence: from physiology to pathology. Nat. Rev. Mol. Cell Biol. *15*, 482–496. https://doi.org/10.1038/nrm3823.
9. Collado, M., Gil, J., Efeyan, A., Guerra, C., Schuhmacher, A.J., Barradas, M., Benguría, A., Zaballos, A., Flores, J.M., Barbacid, M., et al. (2005). Tumour biology: senescence in premalignant tumours. Nature *436*, 642. https://doi.org/10.1038/436642a.
10. Yue, Z., Nie, L., Zhao, P., Ji, N., Liao, G., and Wang, Q. (2022). Senescence-associated secretory phenotype and its impact on oral immune homeostasis. Front. Immunol. *13*, 1019313. https://doi.org/10.3389/fimmu.2022.1019313.
11. Wang, L., Lankhorst, L., and Bernards, R. (2022). Exploiting senescence for the treatment of cancer. Nat. Rev. Cancer *22*, 340–355. https://doi.org/10.1038/s41568-022-00450-9.
12. Guillon, J., Petit, C., Toutain, B., Guette, C., Lelièvre, E., and Coqueret, O. (2019). Chemotherapy-induced senescence, an adaptive mechanism driving resistance and tumor heterogeneity. Cell Cycle *18*, 2385–2397. https://doi.org/10.1080/15384101.2019.1652047.
13. Guccini, I., Revandkar, A., D'Ambrosio, M., Colucci, M., Pasquini, E., Mosole, S., Troiani, M., Brina, D., Sheibani-Tezerji, R., Elia, A.R., et al. (2021). Senescence Reprogramming by TIMP1 Deficiency Promotes Prostate Cancer Metastasis. Cancer Cell *39*, 68–82.e9. https://doi.org/10.1016/j.ccell.2020.10.012.

14. Carver, B.S., Tran, J., Gopalan, A., Chen, Z., Shaikh, S., Carracedo, A., Alimonti, A., Nardella, C., Varmeh, S., Scardino, P.T., et al. (2009). Aberrant ERG expression cooperates with loss of PTEN to promote cancer progression in the prostate. Nat. Genet. *41*, 619–624. https://doi.org/10.1038/ng.370.

15. Calcinotto, A., and Alimonti, A. (2017). Aging tumour cells to cure cancer: "pro-senescence" therapy for cancer. Swiss Med. Wkly. *147*, w14367. https://doi.org/10.57187/smw.2017.14367.

16. Nardella, C., Clohessy, J.G., Alimonti, A., and Pandolfi, P.P. (2011). Pro-senescence therapy for cancer treatment. Nat. Rev. Cancer *11*, 503–511. https://doi.org/10.1038/nrc3057.

17. Leite de Oliveira, R., and Bernards, R. (2018). Anti-cancer therapy: senescence is the new black. EMBO J. *37*, e99386. https://doi.org/10.15252/embj.201899386.

18. Kalathur, M., Toso, A., Chen, J., Revandkar, A., Danzer-Baltzer, C., Guccini, I., Alajati, A., Sarti, M., Pinton, S., Brambilla, L., et al. (2015). A chemogenomic screening identifies CK2 as a target for pro-senescence therapy in PTEN-deficient tumours. Nat. Commun. *6*, 7227. https://doi.org/10.1038/ncomms8227.

19. Tang, X.H., and Gudas, L.J. (2011). Retinoids, retinoic acid receptors, and cancer. Annu. Rev. Pathol. *6*, 345–364. https://doi.org/10.1146/annurev-pathol-011110-130303.

20. Rastinejad, F. (2022). Retinoic acid receptor structures: the journey from single domains to full-length complex. J. Mol. Endocrinol. *69*, T25–T36. https://doi.org/10.1530/JME-22-0113.

21. Duong, V., and Rochette-Egly, C. (2011). The molecular physiology of nuclear retinoic acid receptors. From health to disease. Biochim. Biophys. Acta *1812*, 1023–1031. https://doi.org/10.1016/j.bbadis.2010.10.007.

22. di Masi, A., Leboffe, L., De Marinis, E., Pagano, F., Cicconi, L., Rochette-Egly, C., Lo-Coco, F., Ascenzi, P., and Nervi, C. (2015). Retinoic acid receptors: from molecular mechanisms to cancer therapy. Mol. Aspect. Med. *41*, 1–115. https://doi.org/10.1016/j.mam.2014.12.003.

23. Ghyselinck, N.B., and Duester, G. (2019). Retinoic acid signaling pathways. Development *146*. https://doi.org/10.1242/dev.167502.

24. Quéreux, G., Saint-Jean, M., Peuvrel, L., Brocard, A., Knol, A.C., and Dréno, B. (2013). Bexarotene in cutaneous T-cell lymphoma: third retrospective study of long-term cohort and review of the literature. Expet Opin. Pharmacother. *14*, 1711–1721. https://doi.org/10.1517/14656566.2013.810718.

25. Farol, L.T., and Hymes, K.B. (2004). Bexarotene: a clinical review. Expert Rev. Anticancer Ther. *4*, 180–188. https://doi.org/10.1586/14737140.4.2.180.

26. Waugh, J., Noble, S., and Scott, L.J. (2004). Adapalene: a review of its use in the treatment of acne vulgaris. Drugs *64*, 1465–1478. https://doi.org/10.2165/00003495-200464130-00005.

27. Ramchatesingh, B., Martínez Villarreal, A., Arcuri, D., Lagacé, F., Setah, S.A., Touma, F., Al-Badarin, F., and Litvinov, I.V. (2022). The Use of Retinoids for the Prevention and Treatment of Skin Cancers: An Updated Review. Int. J. Mol. Sci. *23*, 12622. https://doi.org/10.3390/ijms232012622.

28. Rusu, A., Tanase, C., Pascu, G.A., and Todoran, N. (2020). Recent Advances Regarding the Therapeutic Potential of Adapalene. Pharmaceuticals *13*, 217. https://doi.org/10.3390/ph13090217.

29. Pilkington, T., and Brogden, R.N. (1992). Acitretin : A Review of its Pharmacology and Therapeutic Use. Drugs *43*, 597–627. https://doi.org/10.2165/00003495-199243040-00010.

30. Tanaka, T., Suh, K.S., Lo, A.M., and De Luca, L.M. (2007). p21WAF1/CIP1 is a common transcriptional target of retinoid receptors: pleiotropic regulatory mechanism through retinoic acid receptor (RAR)/retinoid X receptor (RXR) heterodimer and RXR/RXR homodimer. J. Biol. Chem. *282*, 29987–29997. https://doi.org/10.1074/jbc.M701700200.

31. Gupta, R., Dong, Y., Solomon, P.D., Wettersten, H.I., Cheng, C.J., Min, J.N., Henson, J., Dogra, S.K., Hwang, S.H., Hammock, B.D., et al. (2014). Synergistic tumor suppression by combined inhibition of telomerase and P21. Proc. Natl. Acad. Sci. USA *111*, E3062–E3071. https://doi.org/10.1073/pnas.1411370111.

32. Wettersten, H.I., Hee Hwang, S., Li, C., Shiu, E.Y., Wecksler, A.T., Hammock, B.D., and Weiss, R.H. (2013). A novel p21 attenuator which is structurally related to sorafenib. Cancer Biol. Ther. *14*, 278–285. https://doi.org/10.4161/cbt.23374.

33. Bolis, M., Bossi, D., Vallerga, A., Ceserani, V., Cavalli, M., Impellizzieri, D., Di Rito, L., Zoni, E., Mosole, S., Elia, A.R., et al. (2021). Dynamic prostate cancer transcriptome analysis delineates the trajectory to disease progression. Nat. Commun. *12*, 7033. https://doi.org/10.1038/s41467-021-26840-5.

34. Muela-Zarzuela, I., Suarez-Rivero, J.M., Gallardo-Orihuela, A., Wan, C., Izawa, K., Gregorio-Procopio, M.d., Coillin, I., Ryffel, B., Kitaura, J., Sanz, A., et al. (2023). NLRP1 inflammasome modulates senescence and senescence-associated secretory phenotype. Preprint at bioRxiv. https://doi.org/10.1101/2023.02.06.527254.

35. Coppé, J.P., Kauser, K., Campisi, J., and Beauséjour, C.M. (2006). Secretion of vascular endothelial growth factor by primary human fibroblasts at senescence. J. Biol. Chem. *281*, 29568–29574. https://doi.org/10.1074/jbc.M603307200.

36. de Groot, I., Brinkman, I., Luijendijk-de Bruin, D., Poort, S., and van Rooijen, J.M. (2021). Docetaxel Treatment for Metastatic Hormone-sensitive Prostate Cancer in Daily Practice. Eur. Urol. Open Sci. *33*, 48–55. https://doi.org/10.1016/j.euros.2021.08.008.

37. James, N.D., Ingleby, F.C., Clarke, N.W., Amos, C.L., Attard, G., Brawley, C.D., Chowdhury, S., Cross, W., Dearnaley, D.P., Gilbert, D.C., et al. (2022). Docetaxel for Nonmetastatic Prostate Cancer: Long-Term Survival Outcomes in the STAMPEDE Randomized Controlled Trial. JNCI Cancer Spectr. *6*, pkac043. https://doi.org/10.1093/jncics/pkac043.

38. Baciarello, G., Delva, R., Gravis, G., Tazi, Y., Beuzeboc, P., Gross-Goupil, M., Bompas, E., Joly, F., Greilsamer, C., Hon, T.N.T., et al. (2022). Patient Preference Between Cabazitaxel and Docetaxel for First-line Chemotherapy in Metastatic Castration-resistant Prostate Cancer: The CABADOC Trial. Eur. Urol. *81*, 234–240. https://doi.org/10.1016/j.eururo.2021.10.016.

39. Di Mitri, D., Toso, A., Chen, J.J., Sarti, M., Pinton, S., Jost, T.R., D'Antuono, R., Montani, E., Garcia-Escudero, R., Guccini, I., et al. (2014). Tumour-infiltrating Gr-1+ myeloid cells antagonize senescence in cancer. Nature *515*, 134–137. https://doi.org/10.1038/nature13638.

40. Chou, T.C. (2010). Drug combination studies and their synergy quantification using the Chou-Talalay method. Cancer Res. *70*, 440–446. https://doi.org/10.1158/0008-5472.CAN-09-1947.

41. Zhang, N., Fu, J.N., and Chou, T.C. (2016). Synergistic combination of microtubule targeting anticancer fludelone with cytoprotective panaxytriol derived from panax ginseng against MX-1 cells in vitro: experimental design and data analysis using the combination index method. Am. J. Cancer Res. *6*, 97–104.

42. Troiani, M., Colucci, M., D'Ambrosio, M., Guccini, I., Pasquini, E., Varesi, A., Valdata, A., Mosole, S., Revandkar, A., Attanasio, G., et al. (2022). Single-cell transcriptomics identifies Mcl-1 as a target for senolytic therapy in cancer. Nat. Commun. *13*, 2177. https://doi.org/10.1038/s41467-022-29824-1.

43. Calcinotto, A., Spataro, C., Zagato, E., Di Mitri, D., Gil, V., Crespo, M., De Bernardis, G., Losa, M., Mirenda, M., Pasquini, E., et al. (2018). IL-23 secreted by myeloid cells drives castration-resistant prostate cancer. Nature *559*, 363–369. https://doi.org/10.1038/s41586-018-0266-0.

44. D'Acquisto, F., Maione, F., and Pederzoli-Ribeil, M. (2010). From IL-15 to IL-33: the never-ending list of new players in inflammation. Is it time to forget the humble aspirin and move ahead? Biochem. Pharmacol. *79*, 525–534. https://doi.org/10.1016/j.bcp.2009.09.015.

45. Tokunaga, R., Zhang, W., Naseem, M., Puccini, A., Berger, M.D., Soni, S., McSkane, M., Baba, H., and Lenz, H.J. (2018). CXCL9, CXCL10, CXCL11/CXCR3 axis for immune activation - A target for novel cancer therapy. Cancer Treat Rev. *63*, 40–47. https://doi.org/10.1016/j.ctrv.2017.11.007.

46. Eferl, R., and Wagner, E.F. (2003). AP-1: a double-edged sword in tumorigenesis. Nat. Rev. Cancer *3*, 859–868. https://doi.org/10.1038/nrc1209.

47. Martínez-Zamudio, R.I., Roux, P.F., de Freitas, J.A.N.L.F., Robinson, L., Doré, G., Sun, B., Belenki, D., Milanovic, M., Herbig, U., Schmitt, C.A., et al. (2020). AP-1 imprints a reversible transcriptional programme of senescent cells. Nat. Cell Biol. *22*, 842–855. https://doi.org/10.1038/s41556-020-0529-5.

48. Jutz, S., Leitner, J., Schmetterer, K., Doel-Perez, I., Majdic, O., Grabmeier-Pfistershammer, K., Paster, W., Huppa, J.B., and Steinberger, P. (2016). Assessment of costimulation and coinhibition in a triple parameter T cell reporter line: Simultaneous measurement of NF-kappaB, NFAT and AP-1. J. Immunol. Methods *430*, 10–20. https://doi.org/10.1016/j.jim.2016.01.007.

49. Izuta, S., Ueki, M., Ueno, M., Nishina, K., Shiozawa, S., and Maekawa, N. (2012). T-5224, a selective inhibitor of c-Fos/activator protein-1, attenuates lipopolysaccharide-induced liver injury in mice. Biotechnol. Lett. *34*, 2175–2182. https://doi.org/10.1007/s10529-012-1022-4.

50. Qi, L., Zhang, Q., Miao, Y., Kang, W., Tian, Z., Xu, D., Xiao, W., and Fang, F. (2020). Interleukin-33 activates and recruits natural killer cells to inhibit pulmonary metastatic cancer development. Int. J. Cancer *146*, 1421–1434. https://doi.org/10.1002/ijc.32779.

51. Ma, S., Caligiuri, M.A., and Yu, J. (2022). Harnessing IL-15 signaling to potentiate NK cell-mediated cancer immunotherapy. Trends Immunol. *43*, 833–847. https://doi.org/10.1016/j.it.2022.08.004.

52. Huntington, N.D., Legrand, N., Alves, N.L., Jaron, B., Weijer, K., Plet, A., Corcuff, E., Mortier, E., Jacques, Y., Spits, H., and Di Santo, J.P. (2009). IL-15 trans-presentation promotes human NK cell development and differentiation in vivo. J. Exp. Med. *206*, 25–34. https://doi.org/10.1084/jem.20082013.

53. Paolini, R., Bernardini, G., Molfetta, R., and Santoni, A. (2015). NK cells and interferons. Cytokine Growth Factor Rev. *26*, 113–120. https://doi.org/10.1016/j.cytogfr.2014.11.003.

54. Krizhanovsky, V., Yon, M., Dickins, R.A., Hearn, S., Simon, J., Miething, C., Yee, H., Zender, L., and Lowe, S.W. (2008). Senescence of activated stellate cells limits liver fibrosis. Cell *134*, 657–667. https://doi.org/10.1016/j.cell.2008.06.049.

55. Quamine, A.E., Olsen, M.R., Cho, M.M., and Capitini, C.M. (2021). Approaches to Enhance Natural Killer Cell-Based Immunotherapy for Pediatric Solid Tumors. Cancers *13*, 2796. https://doi.org/10.3390/cancers13112796.

56. Gorgoulis, V., Adams, P.D., Alimonti, A., Bennett, D.C., Bischof, O., Bishop, C., Campisi, J., Collado, M., Evangelou, K., Ferbeyre, G., et al. (2019). Cellular Senescence: Defining a Path Forward. Cell *179*, 813–827. https://doi.org/10.1016/j.cell.2019.10.005.

57. Toso, A., Revandkar, A., Di Mitri, D., Guccini, I., Proietti, M., Sarti, M., Pinton, S., Zhang, J., Kalathur, M., Civenni, G., et al. (2014). Enhancing chemotherapy efficacy in Pten-deficient prostate tumors by activating the senescence-associated antitumor immunity. Cell Rep. *9*, 75–89. https://doi.org/10.1016/j.celrep.2014.08.044.

58. Chen, Z., Cao, K., Xia, Y., Li, Y., Hou, Y., Wang, L., Li, L., Chang, L., and Li, W. (2019). Cellular senescence in ionizing radiation (Review). Oncol. Rep. *42*, 883–894. https://doi.org/10.3892/or.2019.7209.

59. Sun, Y., Coppé, J.P., and Lam, E.W.F. (2018). Cellular Senescence: The Sought or the Unwanted? Trends Mol. Med. *24*, 871–885. https://doi.org/10.1016/j.molmed.2018.08.002.

60. Cuollo, L., Antonangeli, F., Santoni, A., and Soriani, A. (2020). The Senescence-Associated Secretory Phenotype (SASP) in the Challenging Future of Cancer Therapy and Age-Related Diseases. Biology *9*, 485. https://doi.org/10.3390/biology9120485.

61. Kumari, R., and Jat, P. (2021). Mechanisms of Cellular Senescence: Cell Cycle Arrest and Senescence Associated Secretory Phenotype. Front. Cell Dev. Biol. *9*, 645593. https://doi.org/10.3389/fcell.2021.645593.

62. Liao, Z., Yeo, H.L., Wong, S.W., and Zhao, Y. (2021). Cellular Senescence: Mechanisms and Therapeutic Potential. Biomedicines *9*, 1769. https://doi.org/10.3390/biomedicines9121769.

63. Pasquali, D., Thaller, C., and Eichele, G. (1996). Abnormal level of retinoic acid in prostate cancer tissues. J. Clin. Endocrinol. Metab. *81*, 2186–2191. https://doi.org/10.1210/jcem.81.6.8964849.

64. Ruscetti, M., Leibold, J., Bott, M.J., Fennell, M., Kulick, A., Salgado, N.R., Chen, C.C., Ho, Y.J., Sanchez-Rivera, F.J., Feucht, J., et al. (2018). NK cell-mediated cytotoxicity contributes to tumor control by a cytostatic drug combination. Science *362*, 1416–1422. https://doi.org/10.1126/science.aas9090.

65. Pang, Z., Wang, Z., Li, F., Feng, C., and Mu, X. (2022). Current Progress of CAR-NK Therapy in Cancer Treatment. Cancers *14*, 4318. https://doi.org/10.3390/cancers14174318.

66. Cho, H., Herzka, T., Zheng, W., Qi, J., Wilkinson, J.E., Bradner, J.E., Robinson, B.D., Castillo-Martin, M., Cordon-Cardo, C., and Trotman, L.C. (2014). RapidCaP, a novel GEM model for metastatic prostate cancer analysis and therapy, reveals myc as a driver of Pten-mutant metastasis. Cancer Discov. *4*, 318–333. https://doi.org/10.1158/2159-8290.CD-13-0346.

67. Di Mitri, D., Mirenda, M., Vasilevska, J., Calcinotto, A., Delaleu, N., Revandkar, A., Gil, V., Boysen, G., Losa, M., Mosole, S., et al. (2019). Re-education of Tumor-Associated Macrophages by CXCR2 Blockade Drives Senescence and Tumor Inhibition in Advanced Prostate Cancer. Cell Rep. *28*, 2156–2168.e5. https://doi.org/10.1016/j.celrep.2019.07.068.

68. Livak, K.J., and Schmittgen, T.D. (2001). Analysis of relative gene expression data using real-time quantitative PCR and the 2(-Delta Delta C(T)) Method. Methods *25*, 402–408. https://doi.org/10.1006/meth.2001.1262.

69. Dobin, A., Davis, C.A., Schlesinger, F., Drenkow, J., Zaleski, C., Jha, S., Batut, P., Chaisson, M., and Gingeras, T.R. (2013). STAR: ultrafast universal RNA-seq aligner. Bioinformatics *29*, 15–21. https://doi.org/10.1093/bioinformatics/bts635.

70. Harrow, J., Frankish, A., Gonzalez, J.M., Tapanari, E., Diekhans, M., Kokocinski, F., Aken, B.L., Barrell, D., Zadissa, A., Searle, S., et al. (2012). GENCODE: the reference human genome annotation for The ENCODE Project. Genome Res. *22*, 1760–1774. https://doi.org/10.1101/gr.135350.111.

71. Love, M.I., Huber, W., and Anders, S. (2014). Moderated estimation of fold change and dispersion for RNA-seq data with DESeq2. Genome Biol. *15*, 550. https://doi.org/10.1186/s13059-014-0550-8.

72. Wu, D., and Smyth, G.K. (2012). Camera: a competitive gene set test accounting for inter-gene correlation. Nucleic Acids Res. *40*, e133. https://doi.org/10.1093/nar/gks461.

73. Gillespie, M., Jassal, B., Stephan, R., Milacic, M., Rothfels, K., Senff-Ribeiro, A., Griss, J., Sevilla, C., Matthews, L., Gong, C., et al. (2022). The reactome pathway knowledgebase 2022. Nucleic Acids Res. *50*, D687–D692. https://doi.org/10.1093/nar/gkab1028.

74. Shannon, P., Markiel, A., Ozier, O., Baliga, N.S., Wang, J.T., Ramage, D., Amin, N., Schwikowski, B., and Ideker, T. (2003). Cytoscape: a software environment for integrated models of biomolecular interaction networks. Genome Res. *13*, 2498–2504. https://doi.org/10.1101/gr.1239303.

75. Zheng, G., Tu, K., Yang, Q., Xiong, Y., Wei, C., Xie, L., Zhu, Y., and Li, Y. (2008). ITFP: an integrated platform of mammalian transcription factors. Bioinformatics *24*, 2416–2417. https://doi.org/10.1093/bioinformatics/btn439.

76. Zhao, F., Xuan, Z., Liu, L., and Zhang, M.Q. (2005). TRED: a Transcriptional Regulatory Element Database and a platform for in silico gene regulation studies. Nucleic Acids Res. *33*, D103–D107. https://doi.org/10.1093/nar/gki004.

77. Han, H., Cho, J.W., Lee, S., Yun, A., Kim, H., Bae, D., Yang, S., Kim, C.Y., Lee, M., Kim, E., et al. (2018). TRRUST v2: an expanded reference database of human and mouse transcriptional regulatory interactions. Nucleic Acids Res. *46*, D380–D386. https://doi.org/10.1093/nar/gkx1013.

STAR★METHODS

KEY RESOURCES TABLE

REAGENT or RESOURCE	SOURCE	IDENTIFIER
Antibodies		
InVivo Mab anti-mouse NK1.1	BioXCell	Cat# BE0036; RRID: AB_1107737
Asialo GM1 Polyclonal Antibody	Invitrogen	Cat# 16-6507-39; RRID: AB_10718540
InVivo Mab mouse IgG2a isotype control	BioXCell	Cat# BE0085; RRID: AB_1107771
Donkey anti-Rabbit IgG (H + L) Highly Cross-Adsorbed Secondary Antibody, Alexa Fluor™ 488	Invitrogen	Cat# A-21206; RRID: AB_2535792
Purified anti-mouse CD16/CD32 antibody	BioLegend	Cat# 101302; RRID: AB_312801
CD45 Antibody, anti-mouse, PerCP-Vio® 700, REAfinity	Miltenyi Biotec	Cat# 130-110-801; RRID AB_2658232
APC/Cyanine7 anti-mouse Ly-6G	BioLegend	Cat# 127624; RRID: AB_10640819
Ly-6C Antibody, anti-mouse, PE-Vio® 770, REAfinity	Miltenyi Biotec	Cat# 130-111-918; RRID: AB_2652810
CD11b Antibody, anti-mouse, Vio Bright FITC, REAfinity	Miltenyi Biotec	Cat# 130-113-805; RRID: AB_2726325
CD11b Antibody, anti-mouse, PE-Vio 770, REAfinity	Miltenyi Biotec	Cat# 130-113-808; RRID: AB_2751173
F4/80 Antibody, anti-mouse, APC, REAfinity	Miltenyi Biotec	Cat# 130-116-525; RRID: AB_2733417
CD19 Antibody, anti-mouse, PE, REAfinity	Miltenyi Biotec	Cat# 130-112-035; RRID: AB_2655822
PE anti-mouse CD206 (MMR)	BioLegend	Cat# 141706; RRID: AB_10895754
CD11c Antibody, anti-mouse, VioBlue, REAfinity	Miltenyi Biotec	Cat# 130-110-843; RRID: AB_2654711
Alexa Fluor(R) 488 anti-mouse/human CD45R/B220	BioLegend	Cat# 103225; RRID: AB_389308
CD3 Antibody, anti-mouse, APC-Vio770, REAfinity	Miltenyi Biotec	Cat# 130-119-793; RRID: AB_2751847
CD8 Antibody, anti-mouse, PE-Vio770, REAfinity	Miltenyi Biotec	Cat# 130-119-123; RRID: AB_2733250
CD4 Antibody, anti-mouse, VioBlue, REAfinity	Miltenyi Biotec	Cat# 130-118-696; RRID: AB_2733942
NK1.1 Antibody, anti-mouse, APC, REAfinity	Miltenyi Biotec	Cat# 130-120-507; RRID: AB_2752123
Percp/cy5.5 anti-human CD336 (NKp44)	BioLegend	Cat# 325113; RRID: AB_2616751
Cd335 (NKp46) Rat anti Mouse, Alexa Fluor 647	BD Biosciences	Cat# 560755; RRID: AB_1727464
Anti-Rabbit IgG (H+L), HRP Conjugate	Promega	Cat# W4011; RRID: AB_430833
Anti-Mouse IgG (H+L), HRP Conjugate	Promega	Cat# W4021; RRID: AB_430834
Alexa Fluor® 647 anti-mouse NK-1.1 Antibody	BioLegend	Cat# 108720; RRID: AB_2132713
Cleaved Caspase-3 (Asp175) Antibody	Cell Signaling Technology	Cat# 9661; RRID: AB_2341188
Cleaved Caspase-3 (Asp175) (5A1E) Antibody	Cell Signaling Technology	Cat# 9664; RRID: AB_2070042
p21 Antibody (EPR362)	Abcam	Cat# 109520; RRID: AB_10860537
ALDH1A3 Antibody	Novus Biologicals	Cat# NBP1-91657; RRID: AB_11030810
HSP90 (C45G5) Rabbit mAb	Cell Signaling Technology	Cat# 4877; RRID: AB_2233307
Chemicals, peptides, and recombinant proteins		
Adapalene	MedChem Express	Cat# HY-B0091
Bexarotene	MedChem Express	Cat# HY-14171
Docetaxel	TEVA Pharma AG	
Acitretin	MedChem Express	Cat# HY-B0107
UC2288	MedChem Express	Cat# HY-112780
T-5224	MedChem Express	Cat# HY-12270
c-JUN peptide	Tocris	Cat# 1989
Bovine Pituitary Extract (BPE)	Gibco	Cat# 13028014
Human recombinant Epidermal Growth Factor (EGF)	PeproTech	Cat# AF-100-15
Human recombinant IL-15	PeproTech	Cat# 200-15
Live/Dead staining (Life Technologies	Invitrogen	Cat# L34957
Vitamin A (retinol) (19,19,19,20,20,20-D_6)	Cambridge Isotope Labs	Cat# DLM-8113-0.001
ImProm-II Reverse Transcription System	Promega	Cat# A3800

(*Continued on next page*)

Continued

REAGENT or RESOURCE	SOURCE	IDENTIFIER
RNeasy Mini Kit	Qiagen	Cat# 74106
Gotaq® qPCR Master Mix	Promega	Cat# A6002
Critical commercial assays		
Senescence β-Galactosidase Staining Kit	Cell Signaling	Cat# 9860
Incucyte® Cytotox Green Dye for Counting Dead Cells	Sartorius	Cat# 4633
Incucyte® Caspase-3/7 Dye for Apoptosis	Sartorius	Cat# 4440
Proteome Profiler Mouse XL Cytokine Array	R&D systems	Cat# ARY028
EasySep Human NK Cell Isolation Kit	STEMCELL Technologies	Cat# 17955
NEBNext Ultra Directional RNA Library Prep Kit for Illumina	New England BioLabs Inc.	Cat# E7420
NEBNext® Poly(A) mRNA Magnetic Isolation Module for cDNA synthesis	New England BioLabs Inc.	Cat# E7490
Deposited data		
RNA-seq data on PC3shTIMP1 cells treated with Vehicle, Docetaxel, Adapalene, and Combo	This paper	Gene Expression Omnibus (GEO): GSE253331
Raw data of RNA-seq of human data	Bolis et al. https://doi.org/10.1038/s41467-021-26840-5	https://www.pcaprofiler.com/
Experimental models: Cell lines		
PC3	ATCC	Cat# CRL-1435; RRID: CVCL_0035
PC3 shTIMP1	This paper	
TRAMPC1	ATCC	Cat# CRL-2730; RRID: CVCL_3614
RapidCaP	Trotman laboratory	
LNCaP clone FGC	ATCC	Cat# CRL-1740; RRID: CVCL_1379
22RV1	ATCC	Cat# CRL-2505; RRID: CVCL_1045
RWPE-1	ATCC	Cat# CRL-11609; RRID: CVCL_3791
LapC4		RRID:CVCL_4744
HEK-293T (human embryonic kidneys)	ATCC	Cat# CRL-3216; RRID: CVCL_0063
Experimental models: Organisms/strains		
Mouse- C57BL/6N	Charles River	RRID:MGI:2159965
Mouse- NOD-Rag2tm1-IL2rgtm1 (NRG)	Charles River	RRID:IMSR_RJ:NRG
Oligonucleotides		
See Table S1		
Recombinant DNA		
GIPZ Lentiviral TIMP1 shRNA (clone V3LHS_317110	Horizon Discovery	Cat# RHS4430-200284918-V3LHS_317110
human IL12-directed shRNA	Merck	Cat# TRCN0000058758
human IL33-directed shRNA	Merck	Cat# TRCN0000134092
Plasmid Human c-Jun	Addgene	Cat# 187902; RRID:Addgene_187902
Plasmid pSIRV-AP-1-mCherry	Addgene	Cat# 118095; RRID:Addgene_118095
Plasmid PTEN CRISPR/Cas9 KO	Santa Cruz Biotechnology	Cat# sc-422475
pMSCV-CRE-PURO-IRES-GFP	This paper	
pMSCV-PURO-IRES-GFP	This paper	
Plasmid shp21	Merck	TRCN0000040123, TRCN0000040126
Software and algorithms		
Leica Application Suite X (LAS X)	Leica	RRID:SCR_013673
Graphpad Prism v.9	GraphPad by Dotmatics	RRID: SCR_002798
BD FACSDiva software version 8.0.1	BD	RRID: SCR_001456
FIJI 1.53f51	ImageJ	RRID: SCR_002285
FlowJo software	TreeStar	RRID:SCR_008520

(*Continued on next page*)

Continued		
REAGENT or RESOURCE	SOURCE	IDENTIFIER
Thermo Xcalibur	Thermo Scientific	RRID:SCR_014593
FastQC		RRID:SCR_014583
STAR (v.2.7.10a)		RRID:SCR_004463
ggplot2		RRID:SCR_014601
pheatmap		RRID:SCR_016418
Cytoscape (v 3.9.1)		RRID:SCR_003032
Rstudio		RRID:SCR_000432
Adobe Illustrator		RRID:SCR_010279
Other		
JetPRIME	Polyplus transfection	Cat# 114-07
Incucyte S3 *in vitro* system	Essenbioscience	
Incucyte Wound Maker tool	Essenbioscience	Cat# 9600-0012
Fusion Solo S imaging system	Vilber	
NextSeq2000	Illumina	

RESOURCE AVAILABILITY

Lead contact

Further information and requests for resources and reagents should be directed to and will be fulfilled by the lead contact, Andrea Alimonti (andrea.alimonti@ior.usi.ch).

Materials availability

All reagents generated in Alimonti's laboratory used in this study are available from the lead contact with a completed Materials Transfer Agreement.

Data and code availability

This paper analyzes existing, publicly available data. We analyzed existing publicly available PCa patient cohorts through the PCa Profiler tool (https://www.pcaprofiler.com/).

The gene expression datasets generated for this study have been deposited in Gene Expression Omnibus (GEO) under the accession number GSE253331. These data are publicly available as of the date of publication. The accession number is listed in the key resources table.

EXPERIMENTAL MODEL AND STUDY PARTICIPANT DETAILS

Mouse models

All mice were kept under specific pathogen-free conditions in the animal facility of the IRB institute. Experiments were performed according to the state guidelines and approved by the local ethical committee ("Dipartimento della Sanità e Socialità, Esperimenti su animali" Canton Ticino), authorization number TI-51/2018 (Maximum tumor volume authorized = 1500 mm^3, not exceeded). NRG male mice, at 12 weeks of age, were used for subcutaneous cell injection of $2.5x10^6$ PC3 or PC3shTIMP1 cells. C57BL/6 male mice, at 12 weeks of age, were subcutaneously injected with $2.5x10^6$ TrampC1 cells. Mice were randomized into treatment groups when the tumor reached 100 mm^3 and kept under treatment for 50 days (NRG mice) or 30 days (C57BL/6) after injection. For human NK cell infusion experiments, NRG male mice, at 12 weeks of age, were reconstituted by injecting IP $2.5x10^6$ hNK cells for each mouse. Experiments performed on C57BL/6 male mice, at 12 weeks of age, subcutaneously injected with $2.5x10^6$ RapidCap cells were also performed in the animal facility of the Pharmacology Department of the University of Padova, under Italian national and EU directives (2010/63/EU) for animal research with protocols approved by the institute Ethical Committee and the Italian Ministry of Health (344/2020-PR approved on10/4/2020).

Prostate cancer cell culture

PC3, LNCaP, 22RV1, and LAPC4 human male prostate cancer cells were purchased from ATCC (Cat. N CRL-1435™, CRL-1740™, CRL-2505™, and CVCL-4744™, respectively: the respective RRID are listed in the key resources table) and were cultured according to the manufacturer's instructions. Cells were cultured in RPMI 1640 supplemented with 10% FBS and 1% Penicillin/Streptomycin (P/S). RWPE-1 human normal prostate epithelial cells were purchased from ATCC (CRL-11609™) and were cultured according to the manufacturer's instructions in Keratinocyte Serum-Free Medium Medium (K-SFM) (17005-042, GIBCO) supplemented with

0.05 mg/ml Bovine Pituitary Extract (BPE), 5 ng/ml human recombinant Epidermal Growth Factor (EGF), and 1% P/S. HEK-293T (human embryonic kidneys, Cat. N CRL-3216™), TrampC1 (Cat. N CRL-2730™), and RWPE-1 (CRL-11609D) cells were obtained from ATCC. RapidCaP cells were provided by Trotman's laboratory.[66] Cells were cultured in DMEM supplemented with 10% FBS and 1% P/S. All cell lines were kept at 37°C in a humidified thermostat with 5% CO_2. Cells were periodically tested negative for Mycoplasma (MycoAlertTM mycoplasma detection kit, LT07-418, LONZA) and were used at early passages in the experiments.

METHOD DETAILS

In vivo treatments

Adapalene (MedChemExpress, HY-B0091) and Bexarotene (MedChemExpress, HY-14171) were administered by oral gavage three days/week at the dose of 20 mg/kg and daily at the dose of 20 mg/kg, respectively. Adapalene was resuspended in DMSO 10%, PEG-400 40%, Tween-80 10%. Docetaxel (TEVA, RDCXVR100800) was administered weekly at the dose of 10 mg/kg by intraperitoneal injection.[13,39,42] For the *in vivo* depletion of NK cells, mice were treated with either 50 μg of anti-NK1.1 (clone BE0036, BioXCell), 100 μg Asialo GM1 Polyclonal Antibody (Invitrogen # 16-6507-39), or the isotype control (C1.18.4, BioXCell) on Mondays, Wednesdays, and Fridays. For the in vivo depletion of CD8 T cells, mice were treated with 200 ug of anti-CD8a (clone 53-6.7, Bio X Cell BE0004-1, RRID AB_1125541) or the isotype control (LTF-2, Bio X Cell BE0090, RRID AB_1107780) on Mondays and Thursdays. The respective RRID of each compound is listed in the key resources table. Mice were monitored for suffering, distress, or weight loss by measuring the total body weight weekly and assessing the behavioral changes every day for the entire duration of the experiment.

Generation of a shTIMP1 human prostate cancer cell line

PC3 cells were infected with the human TIMP1-directed shRNA RHS4430-200284918-V3LHS_317110.[13,42] Briefly, to produce the lentiviral particles, HEK-293T cells were transfected using JetPRIME transfection reagents (JetPRIME, Polyplus transfection, 114-07/712-60) according to the manufacturer's instructions. The respective RRID of each reagent is listed in the key resources table. PC3 cells were infected with the filtered lentiviral supernatant suspension obtained from transfected HEK-293T cells. Infected human prostate cancer cells were subsequently selected using Puromycin (3 μg/ml).

Generation of a shp21 cell line

22RV1 and LNCaP cells were infected with the human p21-directed shRNA (Merk TRCN0000040123, TRCN0000040126). Shortly, HEK-293T cells were transfected using JetPRIME transfection reagents (JetPRIME, Polyplus transfection, 114-07/712-60) following the manufacturer's instructions. 22RV1 and LNCaP cells were infected with the filtered lentiviral supernatant suspension obtained from transfected HEK-293T cells. Infected human prostate cancer cells were subsequently selected using Puromycin (3 μg/ml and 2 μg/ml, respectively).

Generation of a shIL-12 and IL-33 human prostate cancer cell Line

PC3 cells were infected with the human IL12-directed shRNA (Merck, TRCN0000058758) and the human IL-33-directed shRNA (Merck, TRCN0000134092). Briefly, to produce the lentiviral particles, HEK-293T cells were transfected using JetPRIME transfection reagents (JetPRIME, Polyplus transfection, 114-07/712-60) according to the manufacturer's instructions. The respective RRID of each reagent is listed in the key resources table. PC3 cells were infected with the filtered lentiviral supernatant from the transfected HEK-293T cells. PC3 cells were subsequently selected using Puromycin (3 μg/ml).

Generation of a cJUN overexpressing human prostate cancer cell line

PC3 cells were infected with the human c-JUN (Addgene #187902). Briefly, to produce the lentiviral particles, HEK-293T cells were transfected using JetPRIME transfection reagents (JetPRIME, Polyplus transfection, 114-07/712-60) according to the manufacturer's instructions. The respective RRID of each reagent is listed in the key resources table. PC3 cells were infected with the filtered lentiviral supernatant suspension and subsequently selected using Puromycin (3 μg/ml).

Generation of PC3 shTIMP1 with mCherry reporter for AP-1

pSIRV-AP-1-mCherry plasmid (Addgene plasmid 118095) was transfected into HEK-293T cells by using JetPRIME transfection reagents. PC3 shTIMP1 cells were infected with the filtered supernatant suspension. The respective RRID of each reagent is listed in the key resources table. Lentiviral supernatant was collected from the transfected HEK-293T cells. mCherry-positive cells indicate AP-1 binding to the promoter.

Generation of *Pten*$^{-/-}$ TrampC1 murine prostate cancer cell lines

TrampC1 cells were purchased from ATCC and cultured following the manufacturer's instructions (DMEM, 10% heat-inactivated FBS, 1% P/S). The transfection of the PTEN CRISPR/Cas9 KO plasmid (Santa Cruz Biotechnology, sc-422475) was performed using jetPRIME® transfection reagent according to the manufactory protocol at the ratio of 1:2 DNA / jetPRIME®. The respective RRID of each reagent is listed in the key resources table. 24h after transfection, the GFP-transduced cells were sorted in order to obtain a 99% purity and plated as single-cell on 96-well plates. Seven days after cell sorting, the cell colonies were moved into 24-well plates for further expansions.[67]

Generation of mouse embryonic fibroblasts primary cell culture

Primary MEFs were generated from single embryos of the $Pten^{loxP/loxP}$ genotype from a pregnant mouse at 13.5 days post-coitum. Embryos were collected and cultured in DMEM with 10% FBS and 1% P/S.

Generation of $Pten^{-/-}$ MEFs

HEK-293T cells were transfected using JetPRIME® transfection reagents (JetPRIME®, Polyplus transfection, 114-07/712-60) according to the manufacturer's instructions in order to prepare lentiviral particles. Primary MEFs were infected with retroviruses expressing either pMSCV-CRE-PURO-IRES-GFP or pMSCV-PURO-IRES-GFP for 48 h and selected with Puromycin at a concentration of 3μg/ml[13].

In vitro treatments

Docetaxel (TEVA, RDCXVR100800) was used at a concentration of 10nM in PC3, RapidCaP, TrampC1, $TrampC1^{Pten-/-}$ cell lines; Docetaxel was used at the dose of 5nM in 22RV1, at 10nM in PC3, and 1 nM in PC3 shTIMP1 cells; Adapalene (MedChemExpress HY-B0091) and Bexarotene (MedChemExpress, HY-14171) were used at a concentration of 10μM or 5μM; Acitretin was used at the dose of 10μM. The p21 inhibor UC2288 (MedChemExpress HY-112780) was used at a concentration of 10μM or 5μM based on the cell lines. The AP-1 inhibitor T-5224 (MedChemExpress, HY-12270) was used at a concentration of 10μM or 5μM based on the cell lines. The cJUN inhibitor (c-JUN peptide, Biotechne, Cat #: 1989) was used at a concentration of 10μM or 5μM based on the cell lines. The respective RRID of each reagent is listed in the key resources table.

Drug combination assay

The drug combination assay was performed by testing five different concentrations of the two drugs (Adapalene or Bexarotene with Docetaxel). Cell proliferation was assessed after 48h of treatment by Cristal Violet, and the Combination Index (CI) was calculated to determine the extent of drug interaction by using the following formula:

$$Combination\ Index\ (CI) = \frac{D1}{Dx1} + \frac{D2}{Dx2}$$

Where D1 and D2 are the concentrations of drug 1 and drug 2 that, used in combination, produce a certain drug effect, while D *x* 1 and D *x* 2 are the concentrations of the single agents alone required to achieve the same effect. CI equal to 1 indicates an additive effect, CI greater than 1 indicates antagonism, and CI lower than 1 indicates synergism.[40,41]

Immunofluorescence (IF) assay

Tumor tissue samples were fixed overnight in 10% neutral-buffered formalin (Thermo Scientific, Cat No. 5701). Tissues were washed with tap water, processed using ethanol, and embedded in paraffin according to standard protocols. 5μm sections were prepared for antibody detection. IF tissue slides were deparaffinized with a three-step approach. In the first and second steps, the sections were soaked in OTTIX plus solution (Diapath, X0076), for 5 minutes each. In the last step, the slides were immersed in OTTIX shaper solution (Diapath, X0096), for 5 minutes. The solution in excess was drained off, and the slides were washed with ionized water for 5 minutes. For the antigen retrieval, the slides were soaked in a pH 6 Citrate solution in a water bath at 98°C for 20 minutes. The slides were allowed to acclimate at room temperature for 20 minutes, washed twice with 1xPBST for 5 minutes each, and then exposed to the Protein-Block solution (DAKO Agilent technologies, X0909) for 20 minutes at room temperature. Then the sections were incubated for 1h at room temperature, or overnight at 4°C, with suitable primary antibodies prepared in the antibody diluent buffer (Thermo Fisher Scientific, 003118), covered from light to not impair fluorophore-labelled primary antibodies. After incubation, the slides were washed three times with 1xPBST for 10 minutes each and further incubated with the respective anti-rabbit secondary antibody (Invitrogen, A21206 AlexaFluor 488, 1:400) for 30 minutes at room temperature, protected from light. In the meantime, the quenching solution was prepared (Invitrogen, R37630) by mixing Solution A, Solution B, and Solution C in equal parts. After secondary antibody staining, the slides were washed twice with 1xPBST for 10 minutes and exposed to the quenching solution for 7 minutes at room temperature in the dark to reduce the fixative-induced autofluorescence. Lastly, the slides were washed with 1xPBST for 10 minutes in the dark and, after draining out the PBST, incubated with a mounting medium with DAPI (Invitrogen, P36931). Following drying at room temperature, the slides were visualized and captured using Leica Thunder fluorescent microscope and the LAS X software. The respective RRID of each reagent is listed in the key resources table.

Senescence Associated β-Galactosidase (SA-β Gal) assay

For tissue-specific SA-β Gal assay, tumor samples, immediately after harvesting, were stored in OCT and snap frozen at -80°C. The samples were then cut at the cryostat by preparing 4μm sections. Senescence-associated SA-β Gal staining was performed using the Senescence β-Galactosidase Staining Kit (Cell Signaling, Cat. No 9860) according to the manufacturer's instructions. The counterstaining was performed using Eosin (Alcohol-based Diapath, C0352).

For the *in vitro* experiments, SA-β Gal staining was performed using the Senescence β-Galactosidase Staining Kit (Cell Signaling Technology, Cat. No 9860) according to the manufacturer's instructions. The respective RRID of each reagent is listed in the key resources table.

Proliferation and cell death assay

The proliferation assay was performed on PC3, TrampC1, TrampC1$^{Pten-/-}$, RapidCaP, 22RV1, PC3shTIMP1, LAPC4, and LNCaP cell lines by plating 1x10^4 cells per well of a 96-well plate in at least a sextuplicate. Proliferation was monitored and analyzed using the Incucyte S3 *in vitro* system (Essenbioscience). Cytotoxicity assays were performed in identical settings by monitoring and quantifying the green fluorescent signals of Cytotox or Caspase 3/7 dyes (Sartorius, 4633 and 4440, respectively).

Cristal Violet assay

Cell proliferation was evaluated by performing Cristal Violet assay. The cells were washed with 1xPBS, fixed with 10% Formalin (Thermo Fisher Scientific, 5701) for 10 minutes, and then stained with Crystal Violet solution (Sigma, V5265) for 15 minutes. The cells were then washed with MilliQ water to remove Cristal Violet excesses, and then allowed to dry overnight. Representative pictures were generated with an image scanner, and cell-bound crystal violet was then extracted using 10% acetic acid solution on the shaker at room temperature for 20 minutes. Sample absorbance was then measured using a spectrophotometer at 590 nm.

Migration assay

The migration assays were performed in PC3shTIMP1 and RapidCaP cell lines. 20x10^4 cells were plated in each well of a 96-well plate in at least a sextuplicate. The wound was performed using the Incucyte Wound Maker tool (Essenbioscience), and cell migration was monitored and analyzed using the Incucyte S3 *in vitro* system (Essenbioscience).

Invasion assay (Boyden chamber)

To assess cell invasion, 5x10^4 PC3shTIMP1 cells were plated in 8.0μm Boyden chambers (Falcon, 353097) that were then placed in a 24-well plate previously filled with conditioned media from senescent or proliferating cells. The experiment was carried on for 8-16h of incubation and then stopped for Cristal Violet staining. The exact number of cells was seeded in the chambers to normalize the migration assay to cell proliferation.

Conditioned media assay

Cell supernatants were harvested and spun down at 453g for 10 mins. The supernatant was then collected and filtered using 0.22 μm filters. The conditioned media were administered to parental cells 48 hours before performing the proliferation and migration assay. In all the experiments, the conditioned media were normalized based on the number of cells in the well at the moment of harvesting.

Cytokine array

Senescent cells-derived conditioned media was harvested and used for the Cytokine Array. The Protein Profiler Array (R&D systems, ARY028) was used according to the manufacturer's instructions to identify SASP factors released in the media. Analysis was performed using the protein array analyzer (ImageJ).

Co-culture experiments

2'000 RapidCaP cells were plated in 24-well plates. Upon attachment, the cells were treated with either Vehicle, Docetaxel, Adapalene, or the combination of the two drugs (Combo) for 48h. Afterward, the cells were washed twice with 1xPBS, and Td-Tomato-labelled RapidCaP cells (TdTomato$^+$ RapidCaP) were added at 2'000 seeding density. Td-Tomato$^+$ RapidCaP cell proliferation was monitored by analyzing the red fluorescent signal of Td-Tomato with the Incucyte S3 *in vitro* system.

Characterization of the tumor immune microenvironment

Tumors were disaggregated and digested in collagenase D and DNase for 30 min at 37°C to obtain a single-cell suspension. After neutralizing unspecific binding with a CD16/CD32 antibody (clone 93), single-cell suspensions were stained with fixable Live/Dead staining (Life Technologies), followed by incubation with specific monoclonal antibodies diluted 1:100 (primary antibodies directly conjugated) to assess the phenotype. The antibodies used were: CD45 (REA737, Miltenyi Biotec); Ly-6G (1A8, Biolegend); Ly6C (REA796, Miltenyi Biotec), CD11b (REA592, Miltenyi Biotec); F4/80 (REA126, Miltenyi Biotec), CD19 (REA749, Miltenyi Biotec), CD206 (C068C2, Biolegend), CD11c (REA754, Miltenyi Biotec), B220 (RA3-6B2, Biolegend), CD3 (REA641, Miltenyi Biotec), CD8 (REA601, Miltenyi Biotec), CD4 (REA604, Miltenyi Biotec), NK1.1 (REA1162, Miltenyi Biotec), NKp44 (P44-8 BioLegend), NKp46 (29A1.4, BD). For flow gating, we used isotype controls of fluorescence minus one control. All the antibodies were purchased from Miltenyi Biotec or Biolegend. Samples were acquired on a BD Canto-II flow cytometer (BD Biosciences). Data were analyzed using FlowJo software (TreeStar, Ashland, OR). The respective RRID of each reagent is listed in the key resources table.

NK cells isolation and coculture

PBMCs were isolated using Ficoll-Paque PLUS (Cytiva 17-1440-03) density gradient from human buffy coat of healthy donors. Pure and fully functional CD3-CD56$^+$ NK cells were isolated from PBMCs using the EasySep Human NK Cell Isolation Kit (STEMCELL Technologies 17955). Expansion of NK cells *in vitro* was performed using RPMI medium supplemented with β-mercaptoethanol, 10% FBS, P/S, Sodium Pyruvate 1mM, and 10ng/ml human recombinant IL-15 (PeproTech 200-15). Activated NK cells were added in coculture with human prostate cancer cells treated or not with either Adapelene, Docetaxel, or their combination in a 5:1 Effector:Target ratio. After 6h of coculture, NK cells were collected for RT-qPCR to assess NK cells activation. The NK-killing potential

was assessed by monitoring and quantifying the green fluorescent signals of Cytotox or Caspase 3/7 dyes (Sartorius, 4633 and 4440, respectively) with the Incucyte S3 *in vitro* system.

Isotope labeling and targeted Lipidomics

Normal (RWPE-1) and prostate cancer (22Rv1) cell lines were plated to 80% confluence on 10cm dishes and allowed to attach overnight. Next, cells were supplemented with fresh medium containing 10μM D6-labeled Retinol (Cambridge Isotope Labs, DLM-8113-0.001). After 24h of incubation with the labeled compound, lipid extraction was performed with ice-cold methanol in water (Supelco, 106035-1000 and 115333-1000, 80:20 v/v). In detail, after medium aspiration, cells were washed twice with PBS on ice and detached by scraping gently in 1.6ml 80% ice-cold methanol (2x 800μl). Afterwards, cells were transferred to a 5ml Potter-Elvehjem homogenizer on ice and homogenized twice (10 to 20 times each) with a 1-minute break. The homogenate was then transferred to an Eppendorf vial, the pestle was washed with 400μl extraction solvent, and the resulting wash was transferred to the Eppendorf vial as well. The homogeneous suspension (2ml) was left for 15 minutes on ice before centrifuging at 13'000g for 3 minutes at 4°C. Lastly, 1.8 ml of supernatant was collected, transferred to a fresh Eppendorf vial, and stored at -80°C until analyzed. The pellet was kept for protein content measurement. The metabolites Retinol, *all-trans*RA, and *13-cis*RA were quantified by Selected Reaction Monitoring (SRM) based reversed phase capLC-nanoESI-MSMS analysis on a triple-quadrupole type mass spectrometer (TSQ Quantiva, Thermo Fisher Scientific Inc., CA, USA). Acquired SRM data were analyzed using the QuanBrowser module of the Xcalibur software (Thermo Fisher Scientific Inc., CA, USA). For each sample, absolute quantities (concentrations in the extracts as μmol/ ml) of the unlabeled and labeled retinol and retinol metabolites were reported based on the co-analysis of the dilution series of the respective analytes. The determined concentrations of the metabolites were normalized to the protein content of the corresponding sample (protein pellet recovered from the lipid extraction).

Sample preparations and LC-MS methods

ACN protein crash/extraction: cells were treated with the indicated compounds, and the pellets were frozen at -80°C until extraction. Before extracting, the samples were thawed on ice, briefly vortexed, and added 200μl H_2O. Then, the samples were vortexed for 5s, 3x freeze/thaw cycle with liquid N2. The samples were successfully homogenized by vortexing and split immediately into two halves, and one half was stored at -80°C. The remaining 100μl of each cell homogenate was supplemented with 400μl of MeOH, vortexed briefly, and incubated on ice for 30 min. The samples were then centrifuged at +4°C/10min/13.2krpm. Then, from each supernatant, 450μl were transferred to new 1.5ml PP tubes. Supernatants were evaporated under a gentle stream of N2/+30°C. Then, the samples were resolubilized by adding 150μl 25% H_2O/75% MeOH/0.1% FA, following 5s vortex and shaken for 10min/1400rpm/+10°C, and again vortex 5s. After this, the samples were centrifuged for 10min/13.2krpm/+4°C and transferred 145μl of each supernatant to LC-MS vials, cap, and submitted to LC-MS.

LC-HRMS, fullMS1

LC method

LC System: Thermo Vanquish Horizon Binary Pump; Eluents: Solvent A: H2O, formic acid (0.1%). Solvent B: Methanol, formic acid (0.1%); Gradient: Linear, from 75% B to 98% B; LC runtime: 5 minutes; LC column: Waters Premier BEH C18 column (50mmx2.1mm); Flow rate: 1ml/min; Column Tem: 50°C; Autosampler Temp: 10°C; Injection Volume: 2μl.

MS method

Mass Spectrometer: Thermo Q Exactive; Acquisition Mode: full MS; MS1 Resolution: 70'000; Scan range: 200 to 600 m/z; AGC target: 1e6;

LC-HRMS, parallel reaction monitoring (PRM)

LC method

LC System: Thermo Vanquish Horizon Binary Pump; Eluents: Solvent A: H2O, formic acid (0.1%);Solvent B: Methanol, formic acid (0.1%); Gradient: Linear, from 75% B to 98% B; LC runtime: 5 minutes; LC column: Waters Premier BEH C18 column (50mmx2.1mm); Flow rate: 1ml/min; Column Temp: 50°C; Autosampler Temp: 10°C; Injection Volume: 2μl.

MS method

Mass Spectrometer: Thermo Q Exactive; Acquisition Mode: PRM; MS2 Resolution: 17'500; Fragmentation: HCD Fragmentation with normalized stepped collision energy 30 and 40.

Liquid-liquid extraction

Samples were extracted and measured as described in the previous section (100μl of each is left, in 75% MeOH/0.1% FA), thawed on ice, and vortexed. The pellet from previous extraction were added (see 1. ACN protein crash/extraction, above), then added the second half of the lysed cells (see 1. ACN protein crash/extraction, above). Samples were vortexed, short spun 10s/13.2krpm peak, and evaporated under a gentle stream of N2/30°C. 20μl 100mM HCl were added to each evaporation residue and vortexed. Successfully, 150μl MeOH were added, and vortexed 10s, then 500μl MTBE, was added and mixed by vortexing.

The samples were incubated and protected from light for 1h/+25°C/1100rpm after which125μl H_2O was added, then vortexed, and centrifuged for 10min/13.2krp/+4°C. The upper organic phase (about 450 μl) was collected and evaporated under a gentle stream of

N2/30°C, while keeping lower aqueous phases and pellets stored at -80°C. 150μl 75% MeOH/0.1% FA was added, vortexed, shaked at 1400rpm/15min/+15°C, followed by vortexing and centrifuged for 10min/13.2krpm/+4°C. Then, supernatants were transferred (approx. 145μl) to LC-MS vials, cap and submit to LC-MS.

LC-HRMS, fullMS1

Performed as described under 1.1, with the only difference being that the injection volume was increased from 2 to 10μl.

LC-HRMS, parallel reaction monitoring (PRM)

Performed as described under 1.2, with the only difference being that the injection volume was increased from 2 to 10μl.

LC-MS on a triple-quadrupole, selected reaction monitoring (SRM)

LC method: LC System: Thermo Vanquish Horizon Binary Pump; Eluents: Solvent A: H_2O, formic acid (0.1%), Solvent B: Methanol, formic acid (0.1%); Gradient: Linear, from 75% B to 98% B; LC runtime: 5 minutes; LC column: Waters Premier BEH C18 column (50mmx2.1mm); Flow rate: 1ml/min; Column Temp: 50C; Autosampler Temp: 10°C; Injection Volume: 10μl

MS method

Mass Spectrometer: Thermo TSQ Quantiva; Acquisition Mode: selected reaction monitoring (SRM); Q1 Resolution: 0.7; Q3 Resolution: 0.7; Fragmentation: CID fragmentation with argon (1.5mTorr).

Western blot

Prostate tissues, tumour samples, or cells were lysed using 1x RIPA buffer (Cell signaling, 9806) supplemented with Phenylmethanesulfonyl fluoride (PMSF; Millipore Sigma, catalogue 329-98-6) and incubated on ice for 30 mins. Samples were centrifuged at 46357g for 15 mins. Protein concentration was determined with the BCA kit (Thermo Fisher, 23227) according to the manufacturer's instructions. Samples were then subjected to SDS-polyacrylamide gel electrophoresis (SDS-PAGE) and transferred onto a 0.45μm nitrocellulose membrane (Thermo Scientific, 88018). Upon blotting, the membranes were blocked with a 5% BSA solution and further incubated overnight at 4°C with the indicated antibodies. The membranes were then incubated with horseradish peroxidase-conjugated (HRP-linked) anti-rabbit IgG (Promega, Cat#W4011, 1:5000) or anti-mouse IgG (Cell Signaling, W4021, 1:5000) secondary antibodies and developed using enhanced chemiluminescence (ECL) substrates (Thermo Scientific, 32106) with Fusion Solo S imaging system (Vilber). Blots were semi-quantitatively analyzed by densitometry using ImageJ 1.52v (National Institutes of Health).

Antibodies

NK-1.1 AlexaFluor 647 BioLegend 108720 1:50 (IF); Cleaved Caspase-3 Cell Signaling Technology 9661 1:1000 (IF); Cleaved Caspase-3 Cell Signaling Technology 9664 1:1000 (WB); p21 Abcam 109520 1:1000 (WB); ALDH1A3 Novus Biologicals NBP1-91657 1:1000 (WB) HSP90 Cell Signaling Technology 4877S 1:1000 (WB). The respective RRID of each reagent is listed in the key resources table.

RNA extraction and RNA sequencing (RNA-seq)

For RT-qPCR, RNA was extracted from cells or tissues using Trizol (Ambion, Life technologies, 15596026) according to the manufacturer's instructions. cDNA was produced using ImProm-II kit (Promega, A3800) according to the manufacturer's instructions. For RNA-seq, RNAs were prepared using RNeasy Mini Kit (Qiagen, 74106), and DNA contaminations were removed with RNase-Free DNase (Qiagen, 79254). NEBNext Ultra Directional RNA Library Prep Kit for Illumina (New England BioLabs Inc.) was used with the NEBNext Multiplex Oligos for Illumina (New England BioLabs Inc.) and NEBNext® Poly(A) mRNA Magnetic Isolation Module for cDNA synthesis; barcode sequences were also included. The sequencing of the prepools was carried out by exploiting the NextSeq2000 (Illumina, San Diego, CA, USA) with the P2 reagents kit V3 (100 cycles; Illumina). Samples were processed starting from stranded, single-ended 120bp-long sequencing reads with the P2 reagents kit V3 (100 cycles; Illumina). Samples were processed starting from stranded, single-ended 120bp-long sequencing reads.

Quantitative real-time PCR (RT-qPCR)

RNA extraction from cells or tissues samples was performed using Trizol (Ambion, Life technologies, 15596026) according to the manufacturer's instructions. cDNA was obtained using ImPROM II kit (Promega, A3800) as reported in the manufacturer's instructions. RT-qPCR was performed using Gotaq® qPCR Master Mix, Promega® (A6002) on Step One Real-Time PCR systems (Applied Biosystems). The respective RRID of each reagent is listed in the key resources table. Primers used for RT-qPCR are listed in Table S1. Expression levels were calculated using the ddCT method.[68]

Bioinformatic analysis

Bulk RNA sequencing was performed on PC3shTIMP1 cells undergoing different treatments: Vehicle, Docetaxel (1nM), Adapalene (5μM), and the combination of Docetaxel and Adapalene.

The tool FastQC (https://www.bioinformatics.babraham.ac.uk/projects/fastqc/) was run to assess the global quality of sequencing reads. Sequences were aligned to the human genome (GRCh38) by exploiting STAR (v.2.7.10a).[69] Transcript quantification was

performed at the gene level by taking advantage of the comprehensive annotations from Gencode.[70] More precisely, we exploited the v39 release of the Gene Transfer File (GTF). We processed the raw counts with R software to perform differential expression analysis by running the DESeq2 package. Genes characterized by zero expression were removed and features with low mean normalized counts were sorted out by Independent Filtering strategy present in DESeq2 (alpha = 0.05).[71] Pathway enrichment analysis of gene lists from RNA-seq was carried out using Camera function[72] on Reactome collection[73] and Hallmark. To perform pathway analysis on custom gene sets, fgsea was also used. The database for secreted factors is derived from the protein atlas secretome (https://www.proteinatlas.org). For the data visualization, all graphs were produced using the ggplot2 package (https://ggplot2.tidyverse.org) and the pheatmap package. Network analysis was performed using Cytoscape (v 3.9.1) with STRING database[74] on transcription factors upregulated in Docetaxel treatment compared to vehicle (FDR<0.05) and downregulated in Combo treatment compared to Docetaxel (FDR<0.05). The human RNA-seq datasets used were obtained from a recent paper by Bolis et al.[33] Pathway analysis of the available gene sets related to the retinoic acid pathway was performed using ss-GSVA scores function (method = ''ssgsea'', ssgsea.norm = TRUE, kcdf = ''Gaussian''). The list of RAR downstream targets was obtained using the tftargets package, particularly combined the targets for RARs from ITFP,[75] TRED,[76] and TTRUST.[77]

QUANTIFICATION AND STATISTICAL ANALYSIS

All experiments were performed in biological replicates, as mentioned in the respective figure legends. All data points are presented for quantitative data, with an overlay of the mean with either SD or SEM. Statistically significant differences between control and experimental groups were determined using simple student's t-tests (two-tailed, unpaired), one-way ANOVA, and two-way ANOVA tests, as indicated in the appropriate figure legends. All statistical analyses were performed using GraphPad Prism 8, or R-Studio.